iScience

CellPress
OPEN ACCESS

Article

Ubiquitin Homeostasis Is Disrupted in TDP-43 and FUS Cell Models of ALS

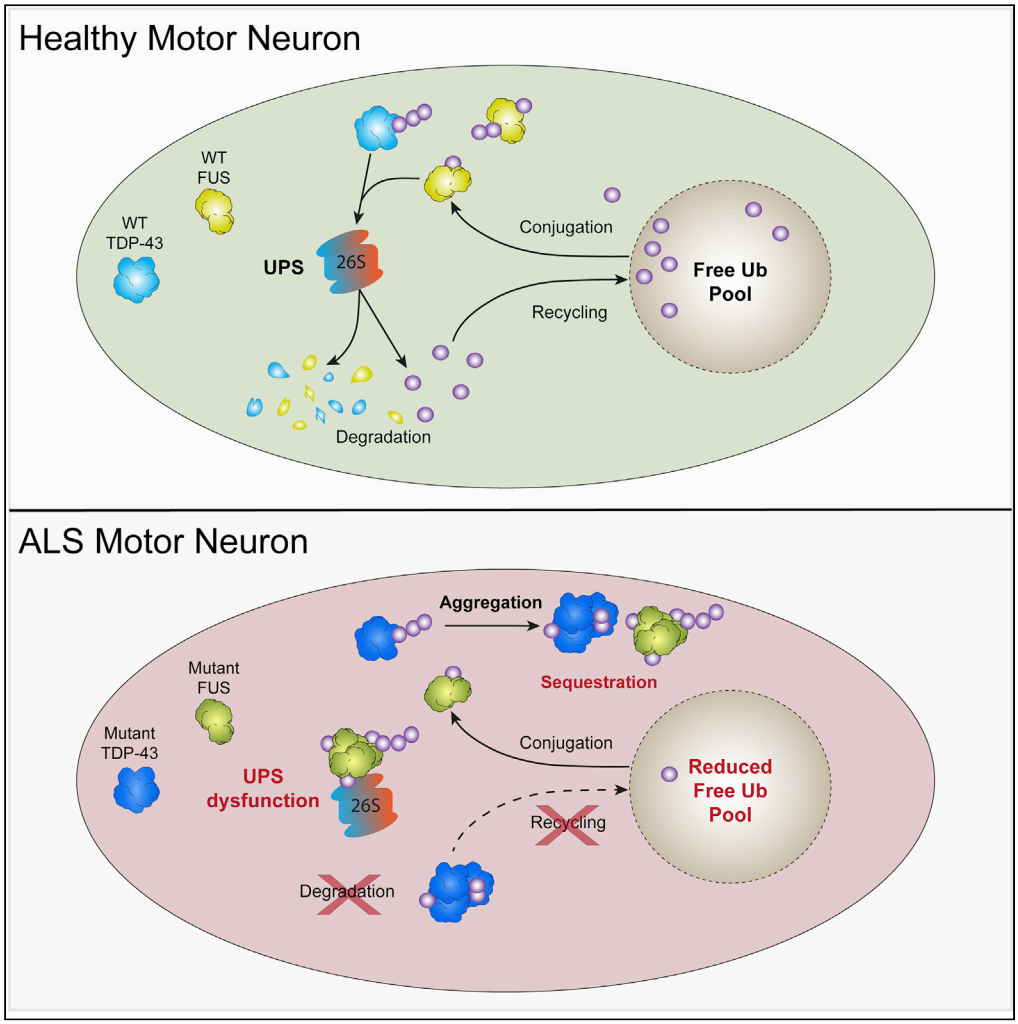

Natalie E. Farrawell, Luke McAlary, Jeremy S. Lum, ..., Kara L. Vine, Darren N. Saunders, Justin J. Yerbury

jyerbury@uow.edu.au

HIGHLIGHTS

The expression of TDP-43^{M337V} and FUS^{R495X} causes UPS dysfunction in NSC-34 cells

The aggregation of TDP-43^{M337V} and FUS^{R495X} depletes the free Ub pool in cells

Ub homeostasis is altered in spinal cord tissue from patients with sALS

Perturbed Ub homeostasis is a common feature of ALS

Farrawell et al., iScience *23*, 101700
November 20, 2020
https://doi.org/10.1016/j.isci.2020.101700

iScience

CellPress
OPEN ACCESS

Article

Ubiquitin Homeostasis Is Disrupted in TDP-43 and FUS Cell Models of ALS

Natalie E. Farrawell,[1,2] Luke McAlary,[1,2] Jeremy S. Lum,[1,2] Christen G. Chisholm,[1,2] Sadaf T. Warraich,[3] Ian P. Blair,[3] Kara L. Vine,[1,2] Darren N. Saunders,[4] and Justin J. Yerbury[1,2,5,*]

SUMMARY

A major feature of amyotrophic lateral sclerosis (ALS) pathology is the accumulation of ubiquitin (Ub) into intracellular inclusions. This sequestration of Ub may reduce the availability of free Ub, disrupting Ub homeostasis and ultimately compromising cellular function and survival. We previously reported significant disturbance of Ub homeostasis in neuronal-like cells expressing mutant SOD1. Here, we show that Ub homeostasis is also perturbed in neuronal-like cells expressing either TDP-43 or FUS. The expression of mutant TDP-43 and mutant FUS led to UPS dysfunction, which was associated with a redistribution of Ub and depletion of the free Ub pool. Redistribution of Ub is also a feature of sporadic ALS, with an increase in Ub signal associated with inclusions and no compensatory increase in Ub expression. Together, these findings suggest that alterations to Ub homeostasis caused by the misfolding and aggregation of ALS-associated proteins play an important role in the pathogenesis of ALS.

INTRODUCTION

Amyotrophic lateral sclerosis (ALS) is a devastating neurodegenerative disease characterized by the progressive loss of motor neurons in the spinal cord and motor cortex, resulting in paralysis and eventually death typically by respiratory failure (Hardiman et al., 2017). The cause(s) of most cases of ALS remains largely unknown (sporadic ALS; sALS), with only approximately 10% of all cases having a clear inherited genetic cause (familial ALS; fALS). There are now over 25 genes known to be associated with ALS (Nguyen et al., 2018), which can be broadly classified into three functional groups including RNA metabolism, trafficking, and protein degradation that have each been proposed to perturb proteome homeostasis (Yerbury et al., 2020). Mutations in RNA-binding proteins TAR DNA-binding protein 43 (TDP-43) and fused-in-sarcoma (FUS) account for a small proportion of fALS cases (~5%) (Chen et al., 2013). However, the wild-type forms of both TDP-43 and FUS are both strongly associated with the etiology of sALS and frontotemporal dementia (FTD) (Neumann et al., 2006, 2009; Arai et al., 2006; Blair et al., 2010; Lai et al., 2011), suggesting these genes play a pivotal role in disease pathology. A growing list of genes encoding components or regulators of the ubiquitin-proteasome system (UPS) and autophagy implicate defective protein degradation in ALS. Mutations in *VCP* (Johnson et al., 2010), *SQSTM1* (Fecto et al., 2011), *UBQLN2* (Deng et al., 2011), *OPTN* (Maruyama et al., 2010), *TBK1* (Cirulli et al., 2015), *CCNF* (Williams et al., 2016), and *DNAJC7* (Farhan et al., 2020) have all been associated with ALS and are all components of cellular protein degradation machinery.

A hallmark of many neurodegenerative diseases, including FTD and ALS, is the abnormal accumulation of proteins into insoluble aggregates or inclusions (Yerbury et al., 2016). It remains to be determined whether these aggregates are a cause or consequence of disease. Evidence suggests that a correlation exists between aggregate load and motor neuron loss in ALS (Ticozzi et al., 2010; Brettschneider et al., 2014; Giordana et al., 2010), and our previous work has shown that mutant superoxide dismutase 1 (SOD1) aggregation propensity correlates with toxicity in the neuronal-like NSC-34 cells (McAlary et al., 2016). Protein inclusions are heterogeneous in their protein composition and contain not just pathological proteins but also molecular chaperones (Sherman and Goldberg, 2001; Yerbury and Kumita, 2010), UPS components (Huang and Figueiredo-Pereira, 2010), and other proteins susceptible to aggregation (Ciryam et al., 2013, 2015). In ALS, the composition of inclusions varies depending on the ALS subtype (sALS versus fALS) and even the underlying mutated gene itself. For example, a majority of sALS and fALS cases have inclusions positive for TDP-43 (Turner et al., 2013) but not SOD1 or FUS; however, SOD1- or FUS-associated

[1]Illawarra Health and Medical Research Institute, Wollongong, NSW 2522, Australia

[2]Molecular Horizons and School of Chemistry and Molecular Bioscience, Science Medicine and Health Faculty, University of Wollongong, Northfields Avenue, Wollongong, NSW 2522, Australia

[3]Centre for Motor Neuron Disease Research, Department of Biomedical Sciences, Faculty of Medicine, Health and Human Sciences, Macquarie University, Sydney, NSW 2109, Australia

[4]School of Medical Sciences, Faculty of Medicine, UNSW, Sydney, NSW 2052, Australia

[5]Lead Contact

*Correspondence: jyerbury@uow.edu.au

https://doi.org/10.1016/j.isci.2020.101700

fALS cases show exclusive deposition of SOD1 and FUS respectively, with no TDP-43 immunoreactivity. In addition to the variation in composition, there is evidence that these different inclusions form by distinct processes in cells (Farrawell et al., 2015). The deposition of specific pathological proteins in different cases suggests that the cellular toxicity may be a result of the sequestration of vital proteins into the inclusions affecting their normal function. Accordingly, we have shown that the sub-proteome that co-aggregates with SOD1, TDP-43, and FUS is composed of supersaturated proteins (Ciryam et al., 2017), with cellular concentrations that exceed their predicted solubility (Ciryam et al., 2013, 2015). These results are consistent with a collapse in the proteostasis capacity of motor neurons in ALS, which is not surprising given that motor neurons have been shown to be particularly susceptible to UPS stress (Bax et al., 2019). Moreover, motor neurons also have a reduced UPS capacity (Brockington et al., 2013) and a more metastable proteome (Yerbury et al., 2019) when compared with ALS-resistant oculomotor neurons, making them particularly vulnerable.

The sequestration of Ub into inclusions is common to all forms of ALS, regardless of the underlying genetics. Ub is best known for its role in targeting proteins for degradation via the proteasome, but it also plays essential roles in a variety of cellular processes including signal transduction, endocytosis, transcription, and DNA repair (Hershko and Ciechanover, 1998; Chen and Sun, 2009). Ub is covalently linked to target proteins through a highly ordered, three-step enzymatic cascade, with differences in Ub chain length and topology determining the fate of the target protein (Pickart, 2001). Inside cells, Ub exists in a dynamic equilibrium between free unconjugated Ub and Ub conjugated in chains (Dantuma et al., 2006; Groothuis et al., 2006). The pool of free Ub is limited and is maintained through controlling Ub expression and the rates of Ub degradation and by recycling Ub from its target substrates. The availability of Ub is particularly important in neurons as it has been shown to regulate differentiation and many aspects of synaptic function including neurogenesis, neuronal excitability, neurotransmission, and synapse formation and elimination (Bax et al., 2019; Mabb and Ehlers, 2010; Kawabe and Brose, 2011). The sequestration of Ub into inclusions may also reduce the availability of free Ub, which is essential for cellular function and survival (Groothuis et al., 2006; Ben Yehuda et al., 2017).

Recently, we showed altered Ub homeostasis in a mutant SOD1 cell model of ALS (Farrawell et al., 2018). The aggregation of pathogenic $SOD1^{A4V}$ in NSC-34 cells led to alterations in UPS activity and redistribution of Ub, disrupting Ub homeostasis and causing mitochondrial dysfunction. It is not currently known if perturbed Ub homeostasis is common to all forms of ALS. Here, we show that Ub homeostasis is disrupted in multiple cell models of ALS. The expression of the mutant forms of ALS-associated proteins, TDP-43 and FUS, caused UPS dysfunction in cells, which was associated with a redistribution of Ub and decreased levels of free monomeric Ub. Increased levels of Ub were also found to be associated with inclusions in postmortem tissue from patients with sALS, confirming that redistribution of Ub is also a feature of sALS. Importantly, this work highlights that misfolded proteins and aggregates associated with ALS contribute to UPS dysfunction and that Ub homeostasis is a key target for monitoring pathological changes in ALS.

RESULTS

TDP-43 and FUS Aggregates Contain K48 and K63-Linked Ubiquitin Chains

K48- and K63-linked polyubiquitin chains are the two most abundant chain types known to target proteins for degradation by the UPS or direct them for removal by autophagy, respectively. We have previously shown that $SOD1^{A4V}$ aggregates contain both Ub^{K48} and Ub^{K63} chains and that Ub was present from the earliest stages of aggregation (Farrawell et al., 2018), whereas TDP-43 and FUS aggregates are ubiquitinated relatively late by comparison (Farrawell et al., 2015). Here, we show that both $TDP\text{-}43^{M337V}$ aggregates (Figure 1A) and FUS^{R495X} aggregates (Figure 1B) contain both Ub^{K48} and Ub^{K63} polymers. In fact, there was a large amount of overlap between $TDP\text{-}43^{M337V}$ aggregates and both Ub^{K48} and Ub^{K63}, with 60% of the $TDP\text{-}43^{M337V}$ aggregates identified within transfected cells colocalized with Ub^{K48} and 73% of $TDP\text{-}43^{M337V}$ aggregates colocalized with Ub^{K63}. Furthermore, the intensity of Ub^{K48} and Ub^{K63} signal associated with $TDP\text{-}43^{M337V}$ aggregates was significantly higher than the signal observed to be associated with soluble $TDP\text{-}43^{M337V}$ (Figure 1C). In cells containing FUS^{R495X} aggregates, ~ 55% of FUS^{R495X} aggregates were positive for Ub^{K48} or Ub^{K63} and the intensity of Ub^{K48} and Ub^{K63} staining was significantly greater in these aggregates when compared with areas containing soluble FUS (Figure 1D).

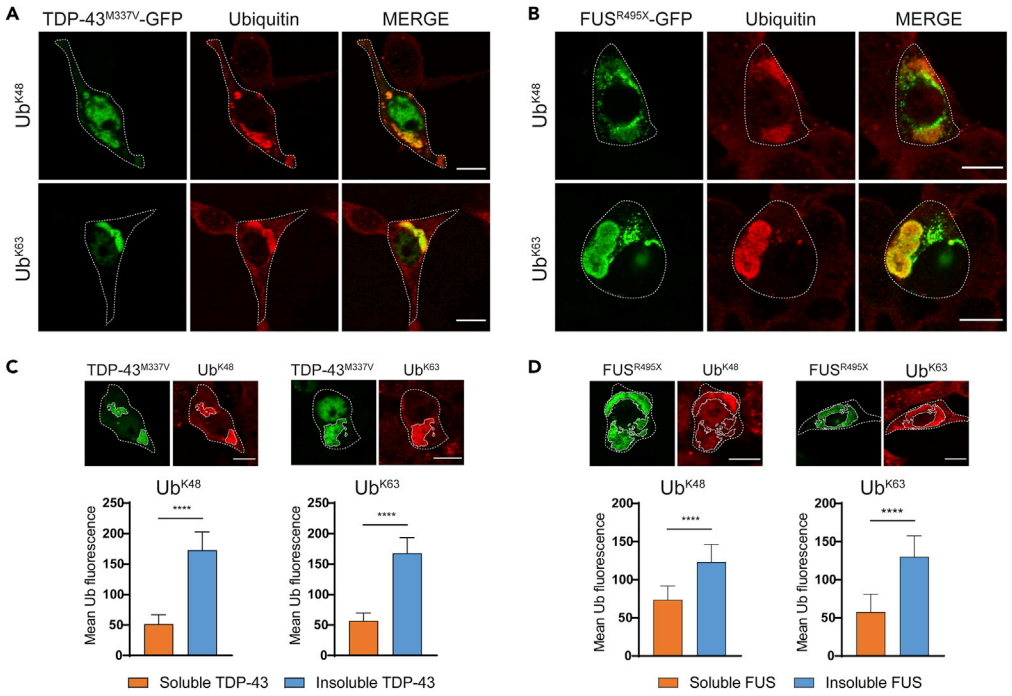

Figure 1. TDP-43 and FUS Aggregates Contain K48 and K63-Linked Ubiquitin Chains

NSC-34 cells transfected with mutant TDP-43-GFP (A) or mutant FUS-GFP (B) were fixed, permeabilized, and stained for Ub^{K48} and Ub^{K63} polymers 48 h post transfection. The mean fluorescence intensity of Ub^{K48} and Ub^{K63} associated with soluble and insoluble TDP-43^{M337V} (C) or FUS^{R495X} (D) was quantified using ImageJ. Data shown are mean ± SD (n = 17 TDP-43/Ub^{K48}, n = 25 TDP-43/Ub^{K63}, n = 19 FUS/Ub^{K48}, n = 25 FUS/Ub^{K63}) and statistical significance between groups was determined using an unpaired Student's t test (****$p < 0.0001$). Scale bars represent 10 μm.

Mutations in TDP-43 and FUS Cause UPS Dysfunction

We have previously shown that cells containing $SOD1^{A4V}$ aggregates have a dysfunctional UPS, as evidenced by the accumulation of significantly higher amounts of the fluorescent UPS reporter $tdTomato^{CL1}$ compared with cells expressing $SOD1^{WT}$ (Farrawell et al., 2018). To investigate whether cells expressing ALS-associated mutant TDP-43 or FUS have a dysfunctional UPS, we co-transfected NSC-34 cells with TDP-43-GFP, FUS-GFP, or tGFP and $tdTomato^{CL1}$ and measured $tdTomato^{CL1}$ accumulation in the presence of increasing concentrations of MG132 by flow cytometry. Cells expressing TDP-43^{WT} and TDP-43^{M337V} showed a dose-dependent increase in $tdTomato^{CL1}$ signal with MG132 treatment, which was significantly higher than the signal observed in cells expressing the tGFP control at all the concentrations tested (Figure 2A). Modest increases in $tdTomato^{CL1}$ signal were observed with increasing MG132 concentrations in cells expressing the tGFP control (Figure S1), suggesting that UPS function was not completely impaired at the concentrations tested. Although cells expressing TDP-43^{M337V} exhibited higher levels of $tdTomato^{CL1}$ fluorescence compared with cells expressing TDP-43^{WT}, this increase was only significant at the highest concentration of MG132 tested. In contrast, cells expressing FUS^{R495X} exhibited significantly higher levels of $tdTomato^{CL1}$ signal than cells expressing FUS^{WT} at all the concentrations tested (Figure 2B). Together, these results suggest that the overexpression of ALS-associated TDP-43 and FUS causes UPS dysfunction.

Ubiquitin Pools Are Disturbed in Cells Expressing ALS Mutants of TDP-43 and FUS

To determine whether the UPS dysfunction observed in cells expressing mutant TDP-43 and mutant FUS was associated with altered Ub homeostasis, we assessed the mobility and distribution of Ub in cells using fluorescence recovery after photo bleaching (FRAP) (Axelrod et al., 1976; Dantuma et al., 2006). By bleaching regions of interest in the nucleus and cytoplasm of cells co-expressing mCherry-Ub and TDP-43-GFP or FUS-GFP (Figure S2), we could measure the recovery of mCherry-Ub into these regions to determine the rate of nucleocytoplasmic Ub diffusion and cellular availability of mobile Ub. In the case of cells expressing

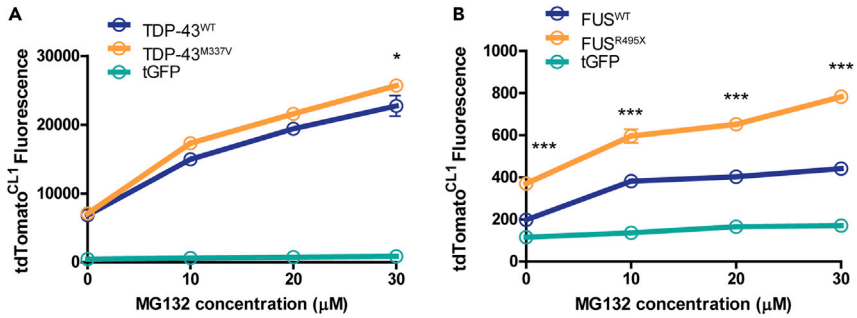

Figure 2. ALS Mutant TDP-43 and ALS Mutant FUS Alter UPS Activity in Living Cells

Dose-dependent response of UPS activity (tdTomato^{CL1} fluorescence) in NSC-34 cells co-transfected with TDP-43-GFP (A) or FUS-GFP (B) after overnight treatment (18 h) with the proteasome inhibitor, MG132. Data represent mean tdTomato^{CL1} fluorescence ±SEM (n = 3) *p < 0.05, ***p < 0.001 indicate significant difference to WT (two-way ANOVA with Bonferroni post-test). See also Figure S1.

mutant TDP-43^{M337V}-GFP, we examined two subpopulations of cells, those expressing soluble TDP-43^{M337V}-GFP and those containing insoluble TDP-43^{M337V}-GFP aggregates (defined as bright fluorescent puncta > 2 μm). This distinction between subpopulations was not made in cells expressing FUS^{R495X}-GFP, as the majority of FUS^{R495X}-GFP mislocalizes to the cytoplasm where it forms small foci and larger aggregates. For this set of experiments, cells containing large FUS^{R495X}-GFP aggregates were selected for FRAP.

Patterns of Ub recovery for cells expressing both TDP-43-GFP (Figure 3A) and FUS-GFP (Figure 3B) were similar to those observed previously with NSC-34 cells expressing SOD1-GFP (Farrawell et al., 2018), in that levels of cytoplasmic recovery were higher than levels of recovery in the nucleus, indicating increased Ub mobility. However, cells expressing soluble TDP-43^{M337V}-GFP appeared to have slightly lower levels of cytoplasmic recovery when compared with other cell populations expressing TDP-43-GFP and the tGFP control (Figure 3A). Cells expressing either FUS^{WT}-GFP or FUS^{R495X}-GFP both had slightly lower levels of cytoplasmic recovery in comparison with the tGFP control (Figure 3B), suggesting differences in the levels of mobile Ub. After calculating the mean half-life of recovery ($T_{1/2}$), significant increases were observed in the cytoplasm of cells containing insoluble TDP-43^{M337V}-GFP and in the nucleus of cells expressing FUS^{WT}-GFP when compared with the relevant tGFP control (Figure 3C), suggesting that the kinetics of Ub diffusion is altered in these cells (presumably as Ub is being incorporated into larger complexes). When the amount (%) of mobile Ub available to cells was quantified, no significant differences were observed between populations expressing TDP-43-GFP. However, cells expressing both FUS^{WT}-GFP and FUS^{R495X}-GFP had significantly lower levels of mobile Ub in the cytoplasm in comparison with the tGFP control (Figure 3D).

Free Ubiquitin Availability Is Lowered in Cells Expressing ALS Mutants of TDP-43 and FUS

To test whether the expression of TDP-43-GFP and FUS-GFP altered the amount of free monomeric Ub in cells, we fractionated cell lysates of NSC-34 cells expressing either wild-type or mutant TDP-43-GFP and FUS-GFP and analyzed the relative amount of monomeric Ub by western blotting (Figure S3). Similar to our previous findings in SOD1-GFP-transfected cells (Farrawell et al., 2018), we were unable to detect significant differences in free Ub levels using this method, most likely as this analysis represents a measurement of both transfected and non-transfected cells in culture. Therefore, we examined the monomeric Ub pool in cells expressing TDP-43-GFP and FUS-GFP by fluorescence recovery after nuclear photobleaching (FRANP) (Farrawell et al., 2018). Using the nuclear pore as a molecular sieve, we bleached the entire nucleus of cells co-expressing mCherry-Ub and TDP-43-GFP (Figures 4A and S4A) or FUS-GFP (Figures 4B and S4B) and monitored the diffusion of monomeric mCherry-Ub back into the nucleus. We observed a significant decrease in the amount of monomeric Ub available to cells containing insoluble TDP-43^{M337V}-GFP aggregates, but there were no significant differences in the levels of monomeric Ub between cells expressing TDP-43^{WT}-GFP, soluble TDP-43^{M337V}–GFP, and the tGFP control (Figure 4C). A significant decrease in monomeric Ub levels was also observed in cells expressing FUS^{R495X}-GFP in comparison with cells expressing FUS^{WT}-GFP and tGFP (Figure 4C).

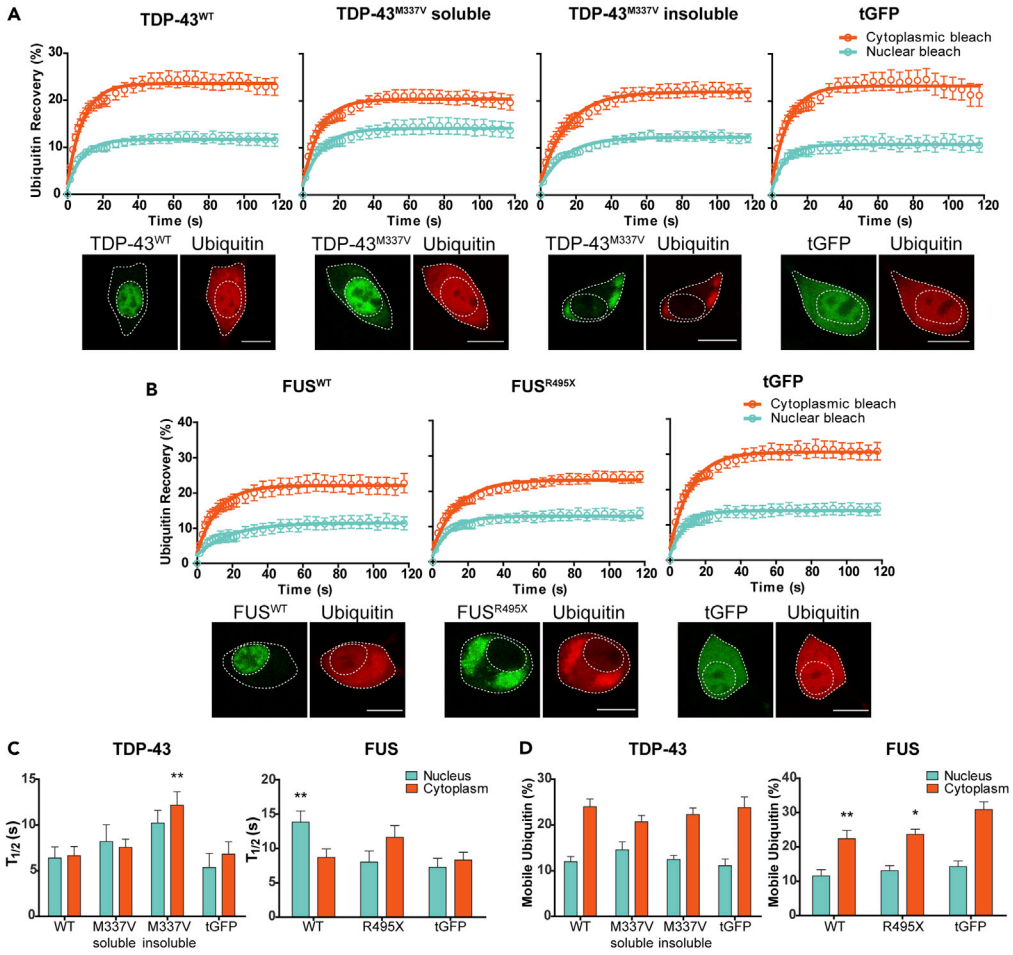

Figure 3. Ubiquitin Distribution Is Altered in Cells Expressing ALS Mutants of TDP-43 and FUS

(A–C) NSC-34 cells co-transfected with TDP-43-GFP (A) or FUS-GFP (B) and mCherry-Ub were photobleached in either the nucleus or cytoplasm and recovery of Ub fluorescence was monitored for 120 s. Data shown are means ± SEM ($n \geq 9$, combined from three independent experiments). Scale bars represent 10 μm. (C) The mean half-life of mCherry-Ub recovery ($T_{1/2}$) was measured in both the nucleus and cytoplasm of NSC-34 cells co-transfected with either TDP-43-GFP or FUS-GFP. Data shown are means ± SEM combined from three independent experiments ($n \geq 9$). Two-way ANOVA with Bonferroni post-test was used to compare differences to the tGFP control (**$p < 0.01$).

(D) Quantification of the proportion of mobile Ub in the nucleus and cytoplasm of cells expressing either TDP-43-GFP or FUS-GFP. Data shown are means ± SEM combined from three independent experiments ($n \geq 9$). *$p < 0.05$, **$p < 0.01$ indicate significant difference to tGFP control (two-way ANOVA with Bonferroni post-test).

See also Figure S2.

To determine whether TDP-43-GFP and FUS-GFP expression also alters the endogenous monomeric Ub pool, we used the probe tUI-HA, which is designed to bind strongly and specifically to free Ub (Choi et al., 2019). Using confocal microscopy, we confirmed the specificity and sensitivity of this probe for free Ub by measuring tUI-HA levels in NSC-34 cells treated with the E1/UBA1 inhibitor TAK-243 (Hyer et al., 2018). We observed a time-dependent increase in tUI-HA fluorescence in cells incubated with the E1 inhibitor compared with cells treated with the DMSO control (Figure S5), consistent with previous reports (Choi et al., 2019) and confirming the specificity of the tUI-HA probe for free Ub. We then measured tUI-HA fluorescence in NSC-34 cells transfected with TDP-43-GFP or FUS-GFP (Figure 5A) and observed a significant reduction in tUI-HA fluorescence in cells expressing TDP-43^{M337V}-GFP or FUS^{R495X}-GFP when compared with cells expressing TDP-43^{WT}-GFP or FUS^{WT}-GFP (Figure 5B). To test whether the aggregation of TDP-43^{M337V}-GFP would also deplete the levels of monomeric Ub available to cells, we manually segregated cells expressing TDP-43^{M337V}-GFP into insoluble and soluble populations before quantifying tUI-HA fluorescence. Cells containing insoluble aggregates of TDP-43^{M337V}-GFP were found to have significantly

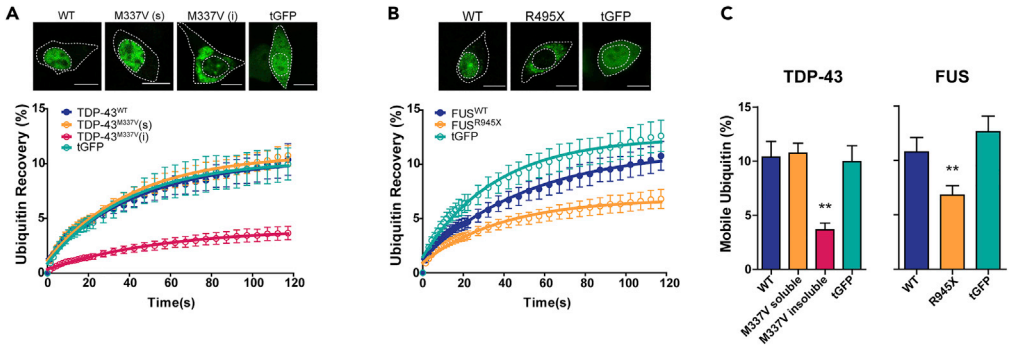

Figure 4. Reduced Levels of Free Monomeric Ubiquitin in NSC-34 Cells Expressing Mutant TDP-43 and Mutant FUS

(A and B) The entire nucleus of NSC-34 cells co-expressing TDP-43-GFP (A) or FUS-GFP (B) and mCherry-Ub was photobleached, and the recovery of nuclear Ub was monitored as a proportion of cytoplasmic fluorescence for 120 s. Data represent mean ± SEM (n ≥ 10 TDP-43, n ≥ 12 FUS, combined from three independent experiments). Scale bars, 10 μm.

(C) The percentage of mobile Ub in the nucleus at the final read was quantified as a proportion of cytoplasmic fluorescence. Data represent mean ± SEM (n ≥ 10 TDP-43, n ≥ 12 FUS, combined from three independent experiments). One-way ANOVA with a Tukey's multiple comparison post-test was used to determine statistical significance compared with tGFP control (**p < 0.01).

See also Figure S4.

lower levels of tUI-HA fluorescence in comparison with cells expressing soluble TDP43^{M337V}-GFP or TDP-43^{WT}-GFP (Figure 5C). These data indicate that the expression and aggregation of mutant TDP-43 and mutant FUS decrease the cellular availability of endogenous free monomeric Ub and are consistent with observations using mCherry labeled Ub reporter (above).

Ubiquitin Homeostasis in ALS Spinal Cord

Inclusions consisting primarily of ubiquitinated and aggregated TDP-43 are a pathological hallmark of sALS. Having shown that the aggregation of TDP-43 in neuronal-like cells resulted in substantial disruption to Ub homeostasis via sequestration of cellular Ub and significant depletion of free monomeric Ub (above), we next sought to interrogate spinal cord motor neurons from sALS postmortem tissue for evidence of perturbed Ub homeostasis. We first probed for both TDP-43 and Ub and confirmed that the distribution of Ub was dispersed evenly throughout spinal cord motor neurons in the absence of TDP-43 inclusions (Figure 6A). In contrast, we observed a significant increase in Ub fluorescence associated with TDP-43 aggregates in cells containing inclusions (Figures 6A, 6B, and S6), consistent with the results of our cell culture models (above). To investigate potential increases in Ub gene expression to compensate for the depletion of free Ub following the accumulation of Ub into inclusions, we analyzed microdissected lumbar spinal cord ventral horn cells from 11 patients with sALS and controls (D'Erchia et al., 2017). Of the four genes encoding Ub (*UBB*, *UBC*, *UBA52*, and *RPS27*), only UBB was significantly reduced in sALS (Figure 6C), but when the expression of all four Ub genes are considered together, there is no overall difference in Ub expression between sALS and controls.

A broader analysis of genes involved in the maintenance of Ub homeostasis (predominantly genes controlling UPS and autophagy) showed significant differences in the relative expression of a number of genes encoding Ub ligases, de-ubiquitinase enzymes (DUBs), and proteases between ALS and control neurons. We observed a pattern of generally decreased expression of UPS genes in ALS (Figure 6D, Tables S1 and S2). We hypothesize that the decrease in expression across the Ub ligases and DUBs, along with the accumulation of Ub chains on soluble and insoluble proteins, would act in concert to reduce the pool of free monomeric Ub in sALS (Figure 6E).

DISCUSSION

Ub is integral to neuronal health and function as it regulates essential cellular processes including protein quality control, protein trafficking, cell cycle regulation, and DNA repair (Hershko and Ciechanover, 1998; Chen and Sun, 2009). The accumulation of Ub-positive inclusions is a hallmark of ALS pathology (Leigh

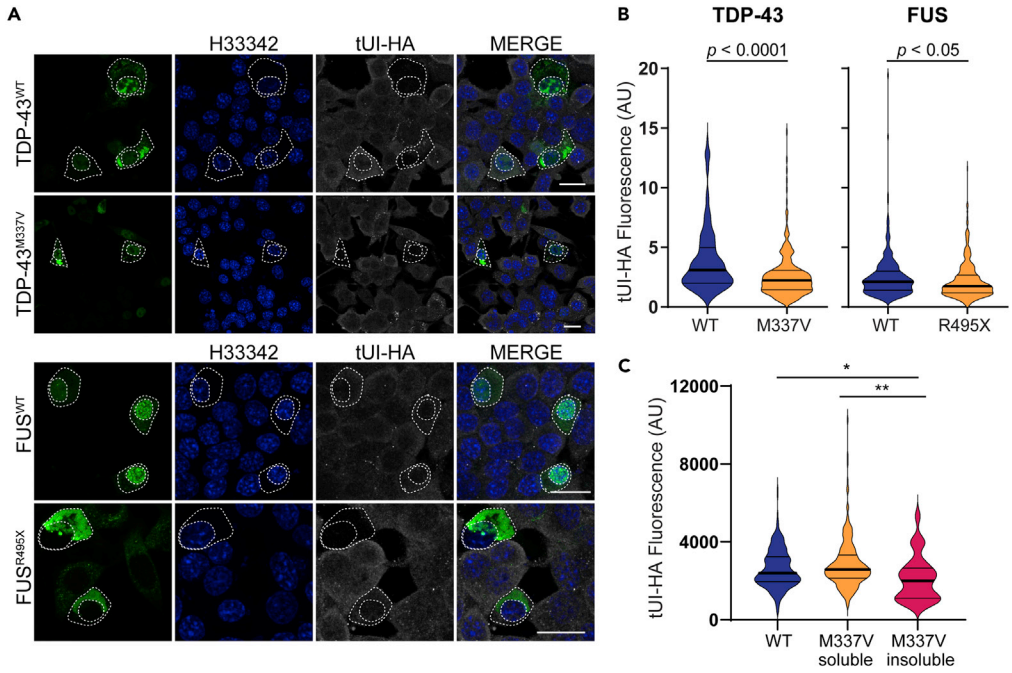

Figure 5. Free Ubiquitin Staining in NSC-34 Cells Expressing TDP-43 and FUS

(A) NSC-34 cells transfected with TDP-43-GFP or FUS-GFP were fixed, permeabilized, and stained for free Ub using the free Ub sensor tUI-HA 48 h post-transfection. Scale bars, 20 μm.

(B) Violin plots of tUI-HA fluorescence in cells expressing either TDP-43-GFP or FUS-GFP calculated from high-throughput image analysis using CellProfiler. Data shown are median, 25th and 75th quartiles with the width of the plot indicating frequency (n = 139 TDP-43^{WT}, n = 253 TDP-43^{M337V}, n = 273 FUS^{WT}, n = 335 FUS^{R495X}). Statistical significance between populations was determined using a Mann-Whitney U test.

(C) Cells expressing TDP-43^{M337V}-GFP were further divided into soluble and insoluble populations via manual segregation, and mean tUI-HA fluorescence was measured in ImageJ. Data are shown as a violin plot with median, 25th-75th quartile and overall data range (n = 250 TDP-43^{WT}, n = 221 TDP-43^{M337V}soluble, n = 27 TDP-43^{M337V}, insoluble). Statistical significance was determined using Kruskal-Wallis test (*p < 0.05, **p < 0.01).

See also Figure S5.

et al., 1991), and the associated sequestration of Ub into inclusions likely disrupts Ub homeostasis by depleting the free Ub pool to levels where cellular functions are severely compromised and ultimately result in cell death. We recently showed that SOD1^{A4V} aggregation caused UPS dysfunction through depletion of the free Ub pool and subsequent disruption of Ub homeostasis (Farrawell et al., 2018). To determine if regulation of Ub homeostasis is perturbed in other models of ALS, we examined the distribution of Ub in cell models expressing ALS-associated proteins TDP-43 and FUS and in spinal cord motor neurons from sALS postmortem tissue. Our results confirm that expression of both mutant TDP-43 and mutant FUS cause UPS dysfunction and alterations to Ub homeostasis. Furthermore, gene expression data from the ventral horn of male patients with ALS suggests that these processes play an important role in the pathogenesis of ALS (D'Erchia et al., 2017).

Ub-mediated protein degradation plays a vital role in maintaining proteostasis (Yerbury et al., 2016), and the UPS has been shown to regulate the levels of ALS-associated proteins in cells (Scotter et al., 2014; Miyazaki et al., 2004), with proteasome inhibition resulting in the accumulation and aggregation of ubiquitinated TDP-43 (Nonaka et al., 2009; van Eersel et al., 2011). Our previous work in NSC-34 cells established that TDP-43 and FUS aggregates accumulate Ub late in comparison with SOD1 aggregates (Farrawell et al., 2015), which contain Ub at the earliest stage of aggregation (Farrawell et al., 2018). Furthermore, we confirmed that SOD1 aggregates contain both K48- and K63-linked polyubiquitin chains, targeting them for degradation by the UPS and/or directing them for removal by autophagy, respectively (Farrawell et al., 2018). In line with these results, we now show that TDP-43 and FUS aggregates contain both K48- and K63-linked polyubiquitin chains. These results are consistent with previous work in human SH-

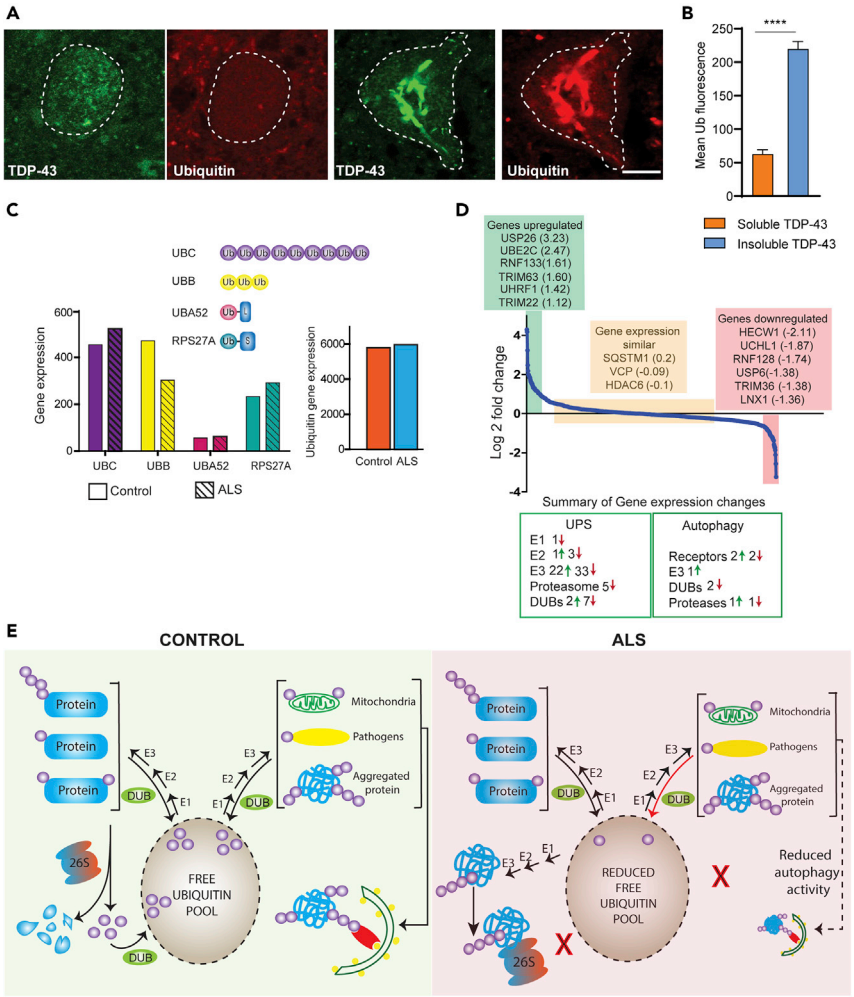

Figure 6. Ubiquitin Homeostasis in sALS

(A) Human ALS postmortem tissue was stained for both TDP-43 and Ub. Inclusions were imaged across two cases of sALS. Representative images of motor neurons with the absence or presence of large skeins that colocalize to Ub staining are shown. Scale bar, 10 μm.

(B) The mean fluorescence intensity of Ub associated with soluble and insoluble TDP-43 was quantified using ImageJ. Data shown are mean ± SD (n = 3) and statistical significance was determined using an unpaired Student's t test (****$p < 0.0001$).

(C) Relative levels of Ub gene expression that were detected in microdissected ventral horn ALS spinal tissue (from D'Erchia et al., 2017).

(D) Waterfall plot of relative expression or fold change of genes in the UPS and autophagy KEGG pathways. Representative genes from three different regions are displayed.

(E) Key processes contributing to free Ub homeostasis and the difference in these processes in ALS compared with control.

See also Figure S6, Tables S1 and S2.

SY5Y cells, which demonstrated that both the UPS and autophagy pathway play a role in the clearance of TDP-43 (Scotter et al., 2014). The presence of both Ub^{K48} and Ub^{K63} linkages suggests that K63 polyubiquitin labeling may be directing aggregates to the Ub-aggresome route when the UPS is inhibited (Yamamoto and Simonsen, 2011). Interestingly, cells expressing mutant FUS have increased levels of Ub^{K48} in comparison with cells expressing FUS^{WT} (Kamelgarn et al., 2018), suggesting a dysfunctional UPS. These results highlight the dependence on tightly regulated Ub homeostasis in neurons and are consistent with the model that mutant ALS-associated proteins compromise UPS function and disrupt Ub homeostasis.

The UPS regulates cellular processes that are fundamental to the structure and function of the nervous system (Mabb and Ehlers, 2010; Chen et al., 2011), and a dysfunctional UPS is thought to contribute to the development of neurodegenerative disorders including ALS. Previously, using the proteasome reporter tdTomato^{CL1}, we have shown that the aggregation of SOD1^{A4V} results in UPS dysfunction in NSC-34 cells. Here, we show that this dysfunction is not specific to SOD1, as an accumulation of tdTomato^{CL1} was observed in cells expressing both TDP-43^{M337V} and FUS^{R495X}. In addition, we found that the levels of UPS dysfunction in cells expressing TDP-43^{M337V} were only significantly different to cells expressing TDP-43^{WT} at the highest concentration of MG132 tested. These results may also be partly explained by the fact that overexpression of TDP-43^{WT} is toxic to cells (Watanabe et al., 2013; Yamashita et al., 2014; Park et al., 2017; Baskaran et al., 2018) and causes motor dysfunction and death in mice (Becker et al., 2017). Furthermore, UPS inhibition causes the aggregation of both TDP-43^{WT} and mutant TDP-43 (Scotter et al., 2014), and the aggregation of TDP-43 leads to the accumulation of the UPS reporter GFP-CL1 in SH-SY5Y cells (Nonaka et al., 2013). The UPS reporter Ub^{G76V}-GFP has also been observed to accumulate in the motor neurons of SOD1^{G93A} mice (Cheroni et al., 2009), highlighting that UPS dysfunction is a common feature of ALS. In fact, UPS dysfunction alone is sufficient to drive ALS pathology, with the motor neuron-specific knockout of the proteasome subunit Rpt3 inducing the aggregation of ALS-associated proteins and motor neuron degeneration in mice (Tashiro et al., 2012).

The aggregation of ALS-associated proteins may exacerbate UPS dysfunction and alter Ub homeostasis in cells by depleting the free Ub pool. We have previously shown that the UPS dysfunction observed in NSC-34 cells containing SOD1^{A4V} aggregates was associated with a redistribution of Ub and decreased levels of free Ub (Farrawell et al., 2018). In this study, we show that the aggregation of mutant TDP-43^{M337V} and mutant FUS^{R495X} also results in changes to Ub homeostasis through the redistribution of Ub and depletion of the free Ub pool. Cellular Ub exists in dynamic pools where free Ub is maintained at an adequate level in order to be able to respond to different cellular conditions (Park and Ryu, 2014). Stress to the proteome causes dramatic changes to the Ub equilibrium by increasing the amount of poly-ubiquitinated protein aggregates and decreasing the free Ub levels in cells (Salomons et al., 2009). Inhibition of the UPS induces similar changes, with MG132 treatment resulting in the accumulation of poly-ubiquitinated proteins and decreased rates of Ub diffusion (Dantuma et al., 2006). Consistent with this, the aggregation of TDP-43^{M337V} and FUS^{R495X} led to changes in the mobility and kinetics of Ub diffusion. Significant changes in Ub mobility were also observed in cells expressing FUS^{WT}, but this is consistent with the fact that the overexpression of FUS^{WT} has been shown to alter the nuclear function of endogenous FUS^{WT} (Sephton et al., 2014) and lead to the accumulation of Ub-positive deposits in mice (Mitchell et al., 2013).

The accumulation of Ub in inclusions is a potential mechanism for Ub depletion, and previous studies have suggested the effects of protein aggregation on Ub homeostasis will be similar regardless of which protein is aggregated (Ben Yehuda et al., 2017). TDP-43 and FUS are both large components of ubiquitinated inclusions in ALS tissue (Arai et al., 2006; Neumann et al., 2006), and here, we confirm through multiple investigations that the aggregation of mutant TDP-43 and mutant FUS deplete the free Ub pool. The consequences of Ub depletion in neurons can be dire, causing defects in neuronal outgrowth and impaired synaptic development (Ryu et al., 2014), which, if prolonged, can lead to cell death. Reduction in cellular Ub levels through disruption to the *UBB* poly-Ub gene gives rise to a progressive neurodegenerative condition in mice (Ryu et al., 2008). Subsequent studies in these *UBB*-deficient mice revealed that compensatory expression from the *UBC* gene is significantly upregulated in an attempt to maintain free Ub levels and protect against neuronal dysfunction (Park et al., 2012). Interestingly, our analysis of spinal cord tissue from patients with sALS revealed that the sequestration of Ub into inclusions was not associated with a compensatory increase in Ub expression. In fact, compared with control tissue, there was a decrease in the expression of *UBB* along with the decreased expression of Ub ligases and DUBs. Modulation of Ub levels can also be achieved through overexpression or removal of Ub from protein aggregates. Overexpression of the DUB USP14 increases the amount of free Ub in cells (Hyrskyluoto et al., 2014), and increasing free Ub levels through Ub overexpression was shown to improve the structural dysfunction in the neuromuscular junction of mice expressing a mutation in USP14 (Vaden et al., 2015). Similarly, an ataxia-associated mutation in the *UCHL1* gene has been associated with decreased levels of monomeric Ub in the brains of mice, and overexpression of UCHL1 results in increased levels of free Ub and improvements in synaptic function (Osaka et al., 2003; Gong et al., 2006). Overexpression

of Ub has also been shown to enhance UPS function and reduce the cytosolic accumulation of TDP-43 and aggregation associated with UBQLN2 overexpression (Picher-Martel et al., 2019). Collectively, these studies demonstrate that modulation of cellular Ub pools play an important role in the pathogenesis of neurodegenerative diseases such as ALS. Moreover, although perturbations to Ub homeostasis appear to be a unifying feature of ALS, it is likely treatment will have to be stratified based on the root cause of the disruption.

In conclusion, we observe that the expression of mutant TDP-43 and mutant FUS causes UPS dysfunction, where the aggregation of these proteins is associated with the redistribution of Ub and depletion of the free Ub pool. Together with our previous observations in a SOD1 model, our findings suggest that perturbations in Ub homeostasis may represent a common molecular pathway underlying neurodegeneration in ALS across genetically distinct forms of the disease.

Limitations of the Study

Although NSC-34 cells exhibit many motor neuron characteristics and are routinely used to model ALS, it should be noted that they are an immortalized mouse cell line. Furthermore, we are using a transient transfection model to ectopically overexpress fluorescently tagged proteins. This type of model recapitulates disease pathology but may not accurately reflect endogenous levels of protein in post-mitotic neurons and restricts the bulk analysis of cell populations (e.g., by western blot), as non-transfected cells influence the results. This work forms the basis of future research using human iPSC-derived motor neurons and animal models to further investigate the importance of Ub homeostasis in ALS.

Resource Availability

Lead Contact

Further information and requests for resources should be directed to the lead contact, Professor Justin Yerbury (jyerbury@uow.edu.au).

Materials Availability

This study did not generate new unique reagents.

Data and Code Availability

Access to data and CellProfiler pipelines can be made available upon reasonable request.

METHODS

All methods can be found in the accompanying Transparent Methods supplemental file.

SUPPLEMENTAL INFORMATION

Supplemental Information can be found online at https://doi.org/10.1016/j.isci.2020.101700.

ACKNOWLEDGMENTS

J.J.Y. was supported by a University of Wollongong Professorship in Neurodegenerative Diseases, and J.J.Y., I.P.B. and N.E.F. were supported by an National Health and Medical Research Council, Australia Dementia Teams Grant (1095215). L.M. was supported by a Motor Neuron Disease Research Institute of Australia Bill Gole Postdoctoral Fellowship. C.G.C was supported by a University of Wollongong-Yerbury Family Scholarship. We thank the New South Wales Brain Bank and Queensland Brain Bank (Australian Brain Bank Network) for access to postmortem tissue.

AUTHOR CONTRIBUTIONS

Conceptualization: N.E.F., D.N.S., J.J.Y.; Methodology: N.E.F., L.M., K.L.V., D.N.S., J.J.Y.; Validation: N.E.F., Formal analysis: N.E.F., L.M., J.S.L., C.G.C., K.L.V., D.N.S., J.J.Y.; Investigation: N.E.F., L.M., J.S.L., S.T.W., D.N.S., J.J.Y.; Resources: D.N.S., J.J.Y.; Data curation: N.E.F., L.M., J.J.Y.; Writing - original draft: N.E.F., J.J.Y.; Writing - review & editing: N.E.F., L.M., J.S.L., C.G.C., I.P.B., K.L.V., D.N.S., J.J.Y.; Visualization: N.E.F., J.J.Y.; Supervision: K.L.V., D.N.S., J.J.Y.; Project administration: K.L.V., J.J.Y.; Funding acquisition: K.L.V., D.N.S., J.J.Y.

DECLARATION OF INTERESTS

The authors declare no competing interests.

Received: August 3, 2020
Revised: September 18, 2020
Accepted: October 14, 2020
Published: November 20, 2020

REFERENCES

Arai, T., Hasegawa, M., Akiyama, H., Ikeda, K., Nonaka, T., Mori, H., Mann, D., Tsuchiya, K., Yoshida, M., Hashizume, Y., and Oda, T. (2006). TDP-43 is a component of ubiquitin-positive tau-negative inclusions in frontotemporal lobar degeneration and amyotrophic lateral sclerosis. Biochem. Biophys. Res. Commun. *351*, 602–611.

Axelrod, D., Koppel, D.E., Schlessinger, J., Elson, E., and Webb, W.W. (1976). Mobility measurement by analysis of fluorescence photobleaching recovery kinetics. Biophys. J. *16*, 1055–1069.

Baskaran, P., Shaw, C., and Guthrie, S. (2018). TDP-43 causes neurotoxicity and cytoskeletal dysfunction in primary cortical neurons. PLoS One *13*, e0196528.

Bax, M., Mckenna, J., Do-Ha, D., Stevens, C.H., Higginbottom, S., Balez, R., Cabral-Da-Silva, M.E.C., Farrawell, N.E., Engel, M., Poronnik, P., et al. (2019). The ubiquitin proteasome system is a key regulator of pluripotent stem cell survival and motor neuron differentiation. Cells *8*, 581.

Becker, L.A., Huang, B., Bieri, G., Ma, R., Knowles, D.A., Jafar-Nejad, P., Messing, J., Kim, H.J., Soriano, A., Auburger, G., et al. (2017). Therapeutic reduction of ataxin-2 extends lifespan and reduces pathology in TDP-43 mice. Nature *544*, 367–371.

Ben Yehuda, A., Risheq, M., Novoplansky, O., Bersuker, K., Kopito, R.R., Goldberg, M., and Brandeis, M. (2017). Ubiquitin accumulation on disease associated protein aggregates is correlated with nuclear ubiquitin depletion, histone de-ubiquitination and impaired DNA damage response. PLoS One *12*, e0169054.

Blair, I.P., Williams, K.L., Warraich, S.T., Durnall, J.C., Thoeng, A.D., Manavis, J., Blumbergs, P.C., Vucic, S., Kiernan, M.C., and Nicholson, G.A. (2010). FUS mutations in amyotrophic lateral sclerosis: clinical, pathological, neurophysiological and genetic analysis. J. Neurol. Neurosurg. Psychiatry *81*, 639–645.

Brettschneider, J., Arai, K., Del Tredici, K., Toledo, J.B., Robinson, J.L., Lee, E.B., Kuwabara, S., Shibuya, K., Irwin, D.J., Fang, L., et al. (2014). TDP-43 pathology and neuronal loss in amyotrophic lateral sclerosis spinal cord. Acta Neuropathol. *128*, 423–437.

Brockington, A., Ning, K., Heath, P.R., Wood, E., Kirby, J., Fusi, N., Lawrence, N., Wharton, S.B., Ince, P.G., and Shaw, P.J. (2013). Unravelling the enigma of selective vulnerability in neurodegeneration: motor neurons resistant to degeneration in ALS show distinct gene expression characteristics and decreased susceptibility to excitotoxicity. Acta Neuropathol. *125*, 95–109.

Chen, P.C., Bhattacharyya, B.J., Hanna, J., Minkel, H., Wilson, J.A., Finley, D., Miller, R.J., and Wilson, S.M. (2011). Ubiquitin homeostasis is critical for synaptic development and function. J. Neurosci. *31*, 17505–17513.

Chen, S., Sayana, P., Zhang, X., and Le, W. (2013). Genetics of amyotrophic lateral sclerosis: an update. Mol. Neurodegener. *8*, 28.

Chen, Z.J., and Sun, L.J. (2009). Nonproteolytic functions of ubiquitin in cell signaling. Mol. Cell *33*, 275–286.

Cheroni, C., Marino, M., Tortarolo, M., Veglianese, P., De Biasi, S., Fontana, E., Zuccarello, L.V., Maynard, C.J., Dantuma, N.P., and Bendotti, C. (2009). Functional alterations of the ubiquitin-proteasome system in motor neurons of a mouse model of familial amyotrophic lateral sclerosis. Hum. Mol. Genet. *18*, 82–96.

Choi, Y.S., Bollinger, S.A., Prada, L.F., Scavone, F., Yao, T., and Cohen, R.E. (2019). High-affinity free ubiquitin sensors for quantifying ubiquitin homeostasis and deubiquitination. Nat. Methods *16*, 771–777.

Cirulli, E.T., Lasseigne, B.N., Petrovski, S., Sapp, P.C., Dion, P.A., Leblond, C.S., Couthouis, J., Lu, Y.F., Wang, Q., Krueger, B.J., et al. (2015). Exome sequencing in amyotrophic lateral sclerosis identifies risk genes and pathways. Science *347*, 1436–1441.

Ciryam, P., Tartaglia, G.G., Morimoto, R.I., Dobson, C.M., and Vendruscolo, M. (2013). Widespread aggregation and neurodegenerative diseases are associated with supersaturated proteins. Cell Rep. *5*, 781–790.

Ciryam, P., Kundra, R., Morimoto, R.I., Dobson, C.M., and Vendruscolo, M. (2015). Supersaturation is a major driving force for protein aggregation in neurodegenerative diseases. Trends Pharmacol. Sci. *36*, 72–77.

Ciryam, P., Lambert-Smith, I.A., Bean, D.M., Freer, R., Cid, F., Tartaglia, G.G., Saunders, D.N., Wilson, M.R., Oliver, S.G., Morimoto, R.I., et al. (2017). Spinal motor neuron protein supersaturation patterns are associated with inclusion body formation in ALS. Proc. Natl. Acad. Sci. U S A *114*, E3935–E3943.

D'Erchia, A.M., Gallo, A., Manzari, C., Raho, S., Horner, D.S., Chiara, M., Valletti, A., Aiello, I., Mastropasqua, F., Ciaccia, L., et al. (2017). Massive transcriptome sequencing of human spinal cord tissues provides new insights into motor neuron degeneration in ALS. Sci. Rep. *7*, 10046.

Dantuma, N.P., Groothuis, T.A., Salomons, F.A., and Neefjes, J. (2006). A dynamic ubiquitin equilibrium couples proteasomal activity to chromatin remodeling. J. Cell Biol. *173*, 19–26.

Deng, H.X., Chen, W., Hong, S.T., Boycott, K.M., Gorrie, G.H., Siddique, N., Yang, Y., Fecto, F., Shi, Y., Zhai, H., et al. (2011). Mutations in UBQLN2 cause dominant X-linked juvenile and adult-onset ALS and ALS/dementia. Nature *477*, 211–215.

Farhan, S.M.K., Howrigan, D.P., Abbott, L.E., Klim, J.R., Topp, S.D., Byrnes, A.E., Churchhouse, C., Phatnani, H., Smith, B.N., Rampersaud, E., et al. (2020). Publisher Correction: Exome sequencing in amyotrophic lateral sclerosis implicates a novel gene, DNAJC7, encoding a heat-shock protein. Nat. Neurosci. *23*, 295.

Farrawell, N.E., Lambert-Smith, I.A., Warraich, S.T., Blair, I.P., Saunders, D.N., Hatters, D.M., and Yerbury, J.J. (2015). Distinct partitioning of ALS associated TDP-43, FUS and SOD1 mutants into cellular inclusions. Sci. Rep. *5*, 13416.

Farrawell, N.E., Lambert-Smith, I., Mitchell, K., Mckenna, J., Mcalary, L., Ciryam, P., Vine, K.L., Saunders, D.N., and Yerbury, J.J. (2018). SOD1(A4V) aggregation alters ubiquitin homeostasis in a cell model of ALS. J. Cell Sci. *131*, jcs209122.

Fecto, F., Yan, J., Vemula, S.P., Liu, E., Yang, Y., Chen, W., Zheng, J.G., Shi, Y., Siddique, N., Arrat, H., et al. (2011). SQSTM1 mutations in familial and sporadic amyotrophic lateral sclerosis. Arch. Neurol. *68*, 1440–1446.

Giordana, M.T., Piccinini, M., Grifoni, S., De Marco, G., Vercellino, M., Magistrello, M., Pellerino, A., Buccinna, B., Lupino, E., and Rinaudo, M.T. (2010). TDP-43 redistribution is an early event in sporadic amyotrophic lateral sclerosis. Brain Pathol. *20*, 351–360.

Gong, B., Cao, Z., Zheng, P., Vitolo, O.V., Liu, S., Staniszewski, A., Moolman, D., Zhang, H., Shelanski, M., and Arancio, O. (2006). Ubiquitin hydrolase Uch-L1 rescues beta-amyloid-induced decreases in synaptic function and contextual memory. Cell *126*, 775–788.

Groothuis, T.A., Dantuma, N.P., Neefjes, J., and Salomons, F.A. (2006). Ubiquitin crosstalk connecting cellular processes. Cell Div. *1*, 21.

Hardiman, O., Al-Chalabi, A., Chio, A., Corr, E.M., Logroscino, G., Robberecht, W., Shaw, P.J., Simmons, Z., and Van Den Berg, L.H. (2017). Amyotrophic lateral sclerosis. Nat. Rev. Dis. Primers *3*, 17085.

Hershko, A., and Ciechanover, A. (1998). The ubiquitin system. Annu. Rev. Biochem. *67*, 425–479.

Huang, Q., and Figueiredo-Pereira, M.E. (2010). Ubiquitin/proteasome pathway impairment in neurodegeneration: therapeutic implications. Apoptosis *15*, 1292–1311.

Hyer, M.L., Milhollen, M.A., Ciavarri, J., Fleming, P., Traore, T., Sappal, D., Huck, J., Shi, J., Gavin, J., Brownell, J., et al. (2018). A small-molecule inhibitor of the ubiquitin activating enzyme for cancer treatment. Nat. Med. *24*, 186–193.

Hyrskyluoto, A., Bruelle, C., Lundh, S.H., Do, H.T., Kivinen, J., Rappou, E., Reijonen, S., Waltimo, T., Petersen, A., Lindholm, D., and Korhonen, L. (2014). Ubiquitin-specific protease-14 reduces cellular aggregates and protects against mutant huntingtin-induced cell degeneration: involvement of the proteasome and ER stress-activated kinase IRE1alpha. Hum. Mol. Genet. *23*, 5928–5939.

Johnson, J.O., Mandrioli, J., Benatar, M., Abramzon, Y., Van Deerlin, V.M., Trojanowski, J.Q., Gibbs, J.R., Brunetti, M., Gronka, S., Wuu, J., et al. (2010). Exome sequencing reveals VCP mutations as a cause of familial ALS. Neuron *68*, 857–864.

Kamelgarn, M., Chen, J., Kuang, L., Jin, H., Kasarskis, E.J., and Zhu, H. (2018). ALS mutations of FUS suppress protein translation and disrupt the regulation of nonsense-mediated decay. Proc. Natl. Acad. Sci. U S A *115*, E11904–E11913.

Kawabe, H., and Brose, N. (2011). The role of ubiquitylation in nerve cell development. Nat. Rev. Neurosci. *12*, 251–268.

Lai, S.L., Abramzon, Y., Schymick, J.C., Stephan, D.A., Dunckley, T., Dillman, A., Cookson, M., Calvo, A., Battistini, S., Giannini, F., et al. (2011). FUS mutations in sporadic amyotrophic lateral sclerosis. Neurobiol. Aging *32*, 550.e1-4.

Leigh, P.N., Whitwell, H., Garofalo, O., Buller, J., Swash, M., Martin, J.E., Gallo, J.M., Weller, R.O., and Anderton, B.H. (1991). Ubiquitin-immunoreactive intraneuronal inclusions in amyotrophic lateral sclerosismorphology, distribution, and specificity. Brain *114*, 775–788.

Mabb, A.M., and Ehlers, M.D. (2010). Ubiquitination in postsynaptic function and plasticity. Annu. Rev. Cell Dev. Biol. *26*, 179–210.

Maruyama, H., Morino, H., Ito, H., Izumi, Y., Kato, H., Watanabe, Y., Kinoshita, Y., Kamada, M., Nodera, H., Suzuki, H., et al. (2010). Mutations of optineurin in amyotrophic lateral sclerosis. Nature *465*, 223–226.

McAlary, L., Aquilina, J.A., and Yerbury, J.J. (2016). Susceptibility of mutant SOD1 to form a destabilized monomer predicts cellular aggregation and toxicity but not in vitro aggregation propensity. Front. Neurosci. *10*, 499.

Mitchell, J.C., Mcgoldrick, P., Vance, C., Hortobagyi, T., Sreedharan, J., Rogelj, B., Tudor, E.L., Smith, B.N., Klasen, C., Miller, C.C., et al. (2013). Overexpression of human wild-type FUS causes progressive motor neuron degeneration in an age- and dose-dependent fashion. Acta Neuropathol. *125*, 273–288.

Miyazaki, K., Fujita, T., Ozaki, T., Kato, C., Kurose, Y., Sakamoto, M., Kato, S., Goto, T., Itoyama, Y., Aoki, M., and Nakagawara, A. (2004). NEDL1, a novel ubiquitin-protein isopeptide ligase for dishevelled-1, targets mutant superoxide dismutase-1. J. Biol. Chem. *279*, 11327–11335.

Neumann, M., Rademakers, R., Roeber, S., Baker, M., Kretzschmar, H.A., and Mackenzie, I.R. (2009). A new subtype of frontotemporal lobar degeneration with FUS pathology. Brain *132*, 2922–2931.

Neumann, M., Sampathu, D.M., Kwong, L.K., Truax, A.C., Micsenyi, M.C., Chou, T.T., Bruce, J., Schuck, T., Grossman, M., Clark, C.M., et al. (2006). Ubiquitinated TDP-43 in frontotemporal lobar degeneration and amyotrophic lateral sclerosis. Science *314*, 130–133.

Nguyen, H.P., Van Broeckhoven, C., and Van Der Zee, J. (2018). ALS genes in the genomic era and their implications for FTD. Trends Genet. *34*, 404–423.

Nonaka, T., Arai, T., Buratti, E., Baralle, F.E., Akiyama, H., and Hasegawa, M. (2009). Phosphorylated and ubiquitinated TDP-43 pathological inclusions in ALS and FTLD-U are recapitulated in SH-SY5Y cells. FEBS Lett. *583*, 394–400.

Nonaka, T., Masuda-Suzukake, M., Arai, T., Hasegawa, Y., Akatsu, H., Obi, T., Yoshida, M., Murayama, S., Mann, D.M., Akiyama, H., and Hasegawa, M. (2013). Prion-like properties of pathological TDP-43 aggregates from diseased brains. Cell Rep. *4*, 124–134.

Osaka, H., Wang, Y.L., Takada, K., Takizawa, S., Setsuie, R., Li, H., Sato, Y., Nishikawa, K., Sun, Y.J., Sakurai, M., et al. (2003). Ubiquitin carboxy-terminal hydrolase L1 binds to and stabilizes monoubiquitin in neuron. Hum. Mol. Genet. *12*, 1945–1958.

Park, C.W., Ryu, H.W., and Ryu, K.Y. (2012). Locus coeruleus neurons are resistant to dysfunction and degeneration by maintaining free ubiquitin levels although total ubiquitin levels decrease upon disruption of polyubiquitin gene Ubb. Biochem. Biophys. Res. Commun. *418*, 541–546.

Park, C.W., and Ryu, K.Y. (2014). Cellular ubiquitin pool dynamics and homeostasis. BMB Rep. *47*, 475–482.

Park, S.K., Hong, J.Y., Arslan, F., Kanneganti, V., Patel, B., Tietsort, A., Tank, E.M.H., Li, X., Barmada, S.J., and Liebman, S.W. (2017). Overexpression of the essential Sis1 chaperone reduces TDP-43 effects on toxicity and proteolysis. PLoS Genet. *13*, e1006805.

Picher-Martel, V., Renaud, L., Bareil, C., and Julien, J.P. (2019). Neuronal expression of UBQLN2(P497H) exacerbates TDP-43 pathology in TDP-43(G348C) mice through Interaction with ubiquitin. Mol. Neurobiol. *56*, 4680–4696.

Pickart, C.M. (2001). Mechanisms underlying ubiquitination. Annu. Rev. Biochem. *70*, 503–533.

Ryu, H.W., Park, C.W., and Ryu, K.Y. (2014). Restoration of cellular ubiquitin reverses impairments in neuronal development caused by disruption of the polyubiquitin gene Ubb. Biochem. Biophys. Res. Commun. *453*, 443–448.

Ryu, K.Y., Garza, J.C., Lu, X.Y., Barsh, G.S., and Kopito, R.R. (2008). Hypothalamic neurodegeneration and adult-onset obesity in mice lacking the Ubb polyubiquitin gene. Proc. Natl. Acad. Sci. U S A *105*, 4016–4021.

Salomons, F.A., Menendez-Benito, V., Bottcher, C., Mccray, B.A., Taylor, J.P., and Dantuma, N.P. (2009). Selective accumulation of aggregation-prone proteasome substrates in response to proteotoxic stress. Mol. Cell. Biol. *29*, 1774–1785.

Scotter, E.L., Vance, C., Nishimura, A.L., Lee, Y.B., Chen, H.J., Urwin, H., Sardone, V., Mitchell, J.C., Rogelj, B., Rubinsztein, D.C., and Shaw, C.E. (2014). Differential roles of the ubiquitin proteasome system and autophagy in the clearance of soluble and aggregated TDP-43 species. J. Cell Sci. *127*, 1263–1278.

Sephton, C.F., Tang, A.A., Kulkarni, A., West, J., Brooks, M., Stubblefield, J.J., Liu, Y., Zhang, M.Q., Green, C.B., Huber, K.M., et al. (2014). Activity-dependent FUS dysregulation disrupts synaptic homeostasis. Proc. Natl. Acad. Sci. U S A *111*, E4769–E4778.

Sherman, M.Y., and Goldberg, A.L. (2001). Cellular defenses against unfolded proteins: a cell biologist thinks about neurodegenerative diseases. Neuron *29*, 15–32.

Tashiro, Y., Urushitani, M., Inoue, H., Koike, M., Uchiyama, Y., Komatsu, M., Tanaka, K., Yamazaki, M., Abe, M., Misawa, H., et al. (2012). Motor neuron-specific disruption of proteasomes, but not autophagy, replicates amyotrophic lateral sclerosis. J. Biol. Chem. *287*, 42984–42994.

Ticozzi, N., Ratti, A., and Silani, V. (2010). Protein aggregation and defective RNA metabolism as mechanisms for motor neuron damage. CNS Neurol. Disord. Drug Targets *9*, 285–296.

Turner, M.R., Hardiman, O., Benatar, M., Brooks, B.R., Chio, A., De Carvalho, M., Ince, P.G., Lin, C., Miller, R.G., Mitsumoto, H., et al. (2013). Controversies and priorities in amyotrophic lateral sclerosis. Lancet Neurol. *12*, 310–322.

Vaden, J.H., Watson, J.A., Howard, A.D., Chen, P.C., Wilson, J.A., and Wilson, S.M. (2015). Distinct effects of ubiquitin overexpression on NMJ structure and motor performance in mice expressing catalytically inactive USP14. Front. Mol. Neurosci. *8*, 11.

van Eersel, J., Ke, Y.D., Gladbach, A., Bi, M., Gotz, J., Kril, J.J., and Ittner, L.M. (2011). Cytoplasmic accumulation and aggregation of TDP-43 upon proteasome inhibition in cultured neurons. PLoS One *6*, e22850.

Watanabe, S., Kaneko, K., and Yamanaka, K. (2013). Accelerated disease onset with stabilized familial amyotrophic lateral sclerosis (ALS)-linked mutant TDP-43 proteins. J. Biol. Chem. *288*, 3641–3654.

Williams, K.L., Topp, S., Yang, S., Smith, B., Fifita, J.A., Warraich, S.T., Zhang, K.Y., Farrawell, N., Vance, C., Hu, X., et al. (2016). CCNF mutations in amyotrophic lateral sclerosis and

frontotemporal dementia. Nat. Commun. *7*, 11253.

Yamamoto, A., and Simonsen, A. (2011). The elimination of accumulated and aggregated proteins: a role for aggrephagy in neurodegeneration. Neurobiol. Dis. *43*, 17–28.

Yamashita, M., Nonaka, T., Hirai, S., Miwa, A., Okado, H., Arai, T., Hosokawa, M., Akiyama, H., and Hasegawa, M. (2014). Distinct pathways leading to TDP-43-induced cellular dysfunctions. Hum. Mol. Genet. *23*, 4345–4356.

Yerbury, J.J., Farrawell, N.E., and Mcalary, L. (2020). Proteome homeostasis dysfunction: a unifying principle in ALS pathogenesis. Trends Neurosci. *43*, 274–284.

Yerbury, J.J., and Kumita, J.R. (2010). Protein chemistry of amyloid fibrils and chaperones: implications for amyloid formation and disease. Curr. Chem. Biol. *4*, 89–98.

Yerbury, J.J., Ooi, L., Dillin, A., Saunders, D.N., Hatters, D.M., Beart, P.M., Cashman, N.R., Wilson, M.R., and Ecroyd, H. (2016). Walking the tightrope: proteostasis and neurodegenerative disease. J. Neurochem. *137*, 489–505.

Yerbury, J.J., Ooi, L., Blair, I.P., Ciryam, P., Dobson, C.M., and Vendruscolo, M. (2019). The metastability of the proteome of spinal motor neurons underlies their selective vulnerability in ALS. Neurosci. Lett. *704*, 89–94.

iScience, Volume *23*

Supplemental Information

Ubiquitin Homeostasis Is Disrupted in TDP-43 and FUS Cell Models of ALS

Natalie E. Farrawell, Luke McAlary, Jeremy S. Lum, Christen G. Chisholm, Sadaf T. Warraich, Ian P. Blair, Kara L. Vine, Darren N. Saunders, and Justin J. Yerbury

Ubiquitin homeostasis is disrupted in TDP-43 and FUS cell models of ALS

SUPPLEMENTAL FIGURES

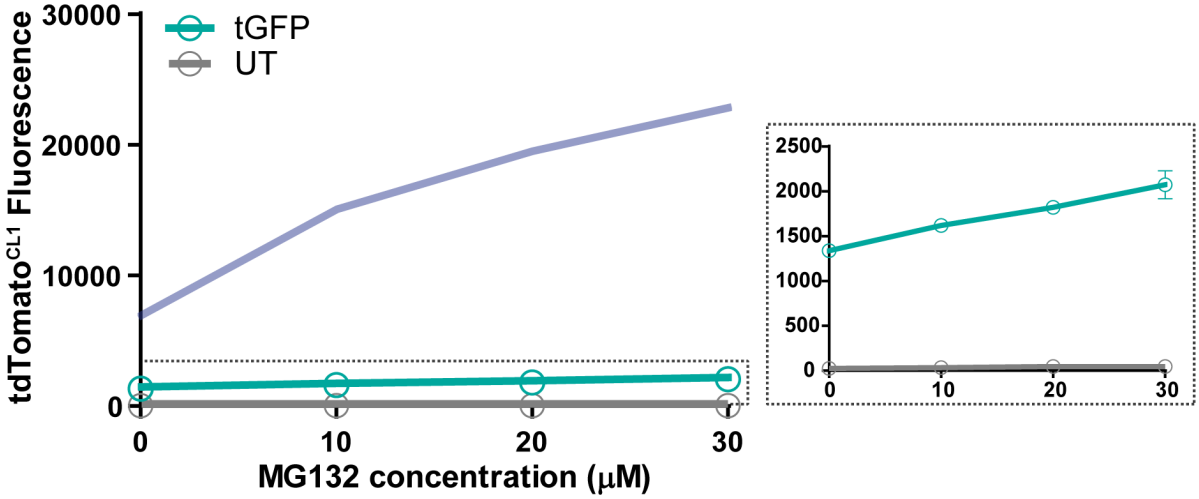

Figure S1. Proteasome inhibition with subinhibitory MG132 treatment has a modest impact on proteasome function in NSC-34 cells expressing tGFP control protein. Related to Figure 2. UPS function was analysed in the untransfected (UT) and GFP positive populations (tGFP) of NSC-34 cells co-transfected with tGFP and the fluorescent UPS reporter tdTomato^{CL1}, after overnight treatment (~18 h) with increasing concentrations (0 - 30 μM) of the proteasome inhibitor MG132. Data represent mean tdTomato^{CL1} fluorescence ± SEM (n=3). The transparent purple line indicates tdTomato^{CL1} fluorescence levels in NSC-34 cells overexpressing TDP-43^{WT}. Right inset displays an increased scale of tdTomato^{CL1} fluorescence to illustrate the differences between the UT and tGFP populations.

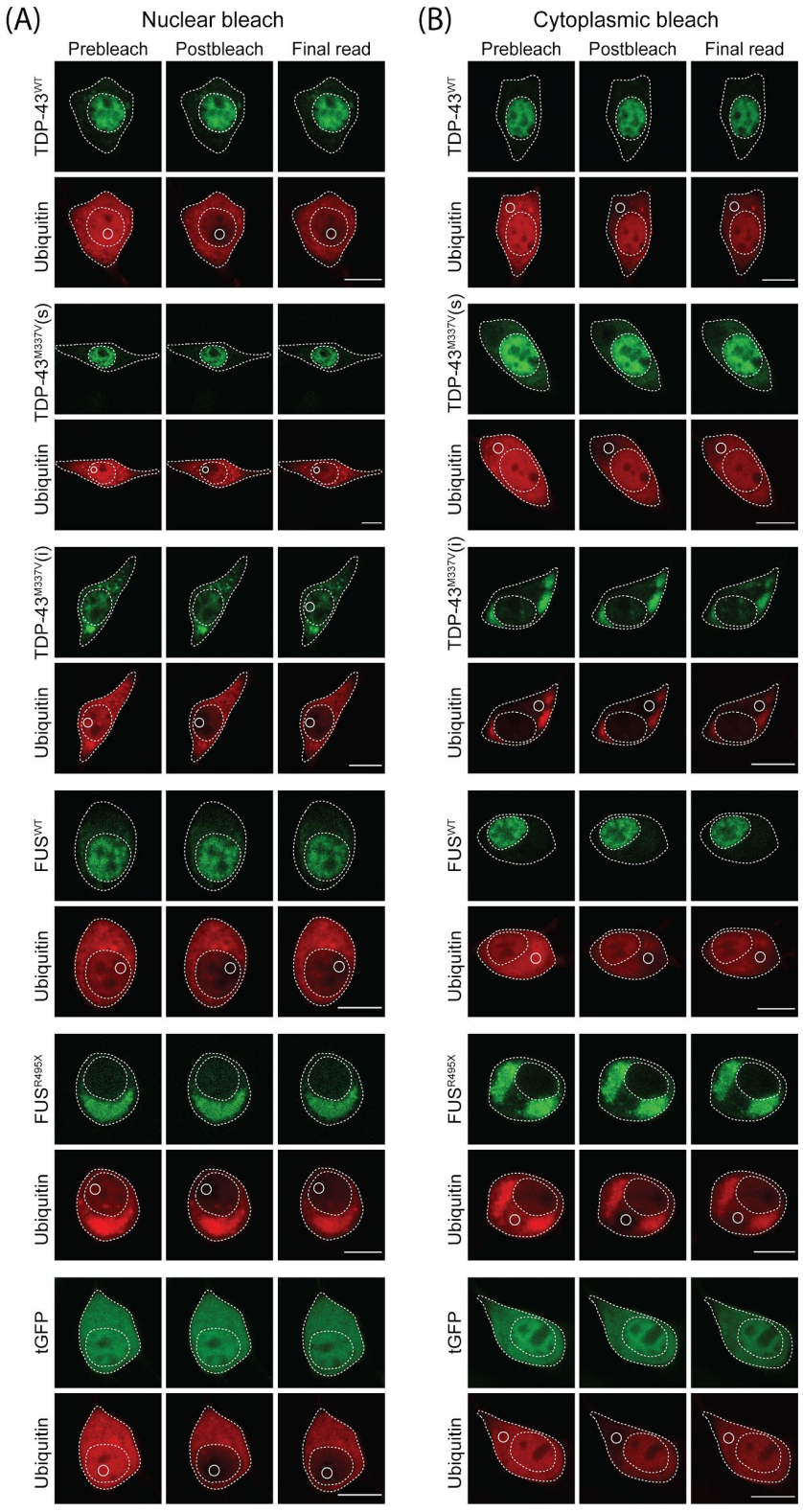

Figure S2. **Representative confocal images of FRAP analysis performed in NSC-34 cells co-expressing mCherry-Ub and TDP-43-GFP or FUS-GFP.** Related to Figure 3. A ROI in the nucleus (A) or cytoplasm (B) of NSC-34 cells co-expressing mCherry-Ub and TDP-43-GFP or FUS-GFP was photobleached and the recovery of Ub fluorescence was monitored. Pre-bleach, post-bleach and recovery endpoint (final read) are shown with the ROI marked by a solid white circle. Scale bars: 10 µm.

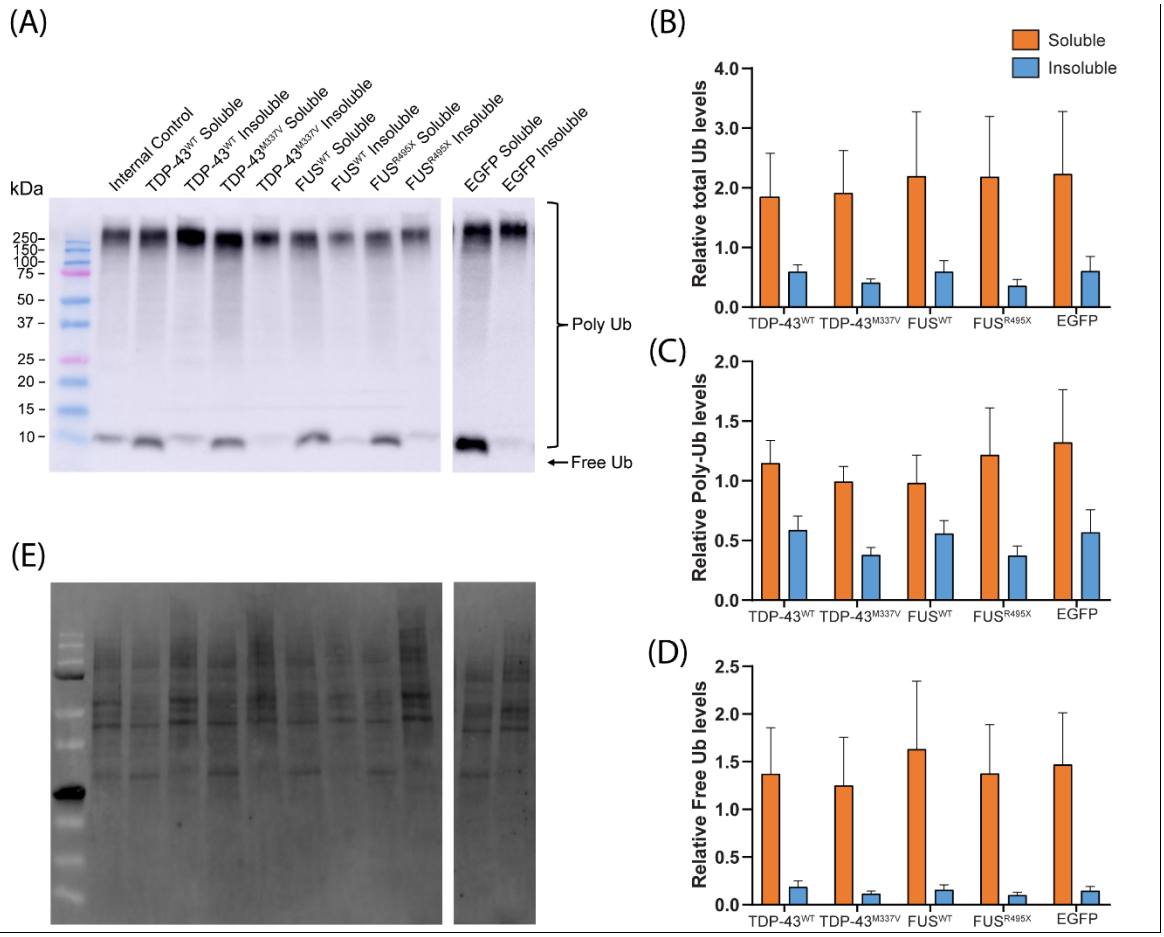

Figure S3. Free ubiquitin levels are not significantly altered in NSC-34 cells containing TDP-43^{M337V} and FUS^{R495X} compared to their WT controls. Related to Figure 4. (A) NSC-34 cells transfected with TDP-43^{WT}-GFP, TDP-43^{M337V}-GFP, FUS^{WT}-GFP, FUS^{R495X}-GFP or EGFP control were lysed in RIPA buffer and soluble and insoluble fractions were analysed for Ub levels by western blot. Quantitative assessment of (B) total Ub, (C) poly-Ub and (D) free Ub levels were analysed compared to (E) total protein using ImageJ software. Data represents mean ± SEM. (n=3 independent biological replicates). A two-way ANOVA (variant x fraction) was performed to compare differences, which were not significant.

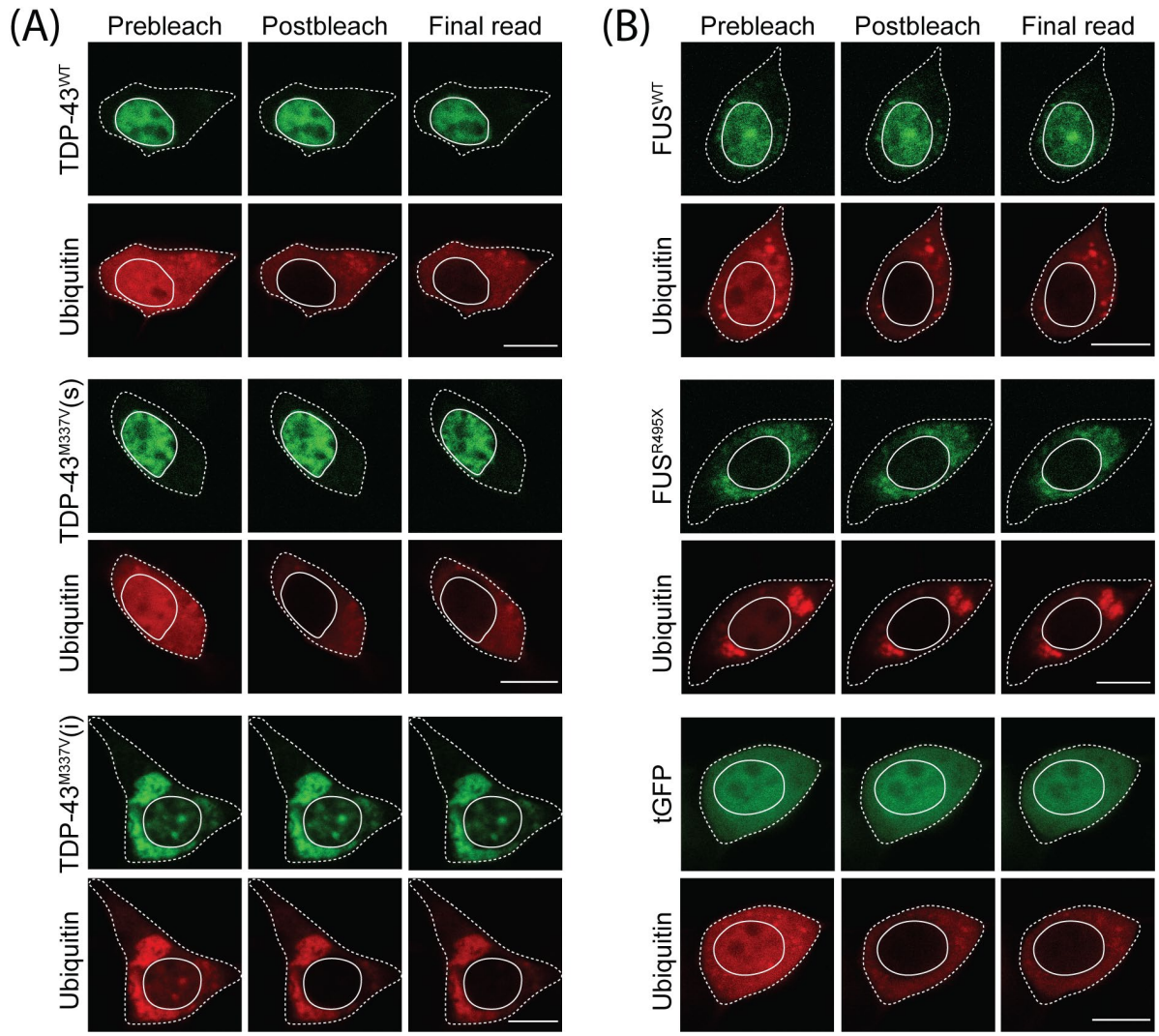

Figure S4. Representative confocal images of FRANP analysis performed on NSC-34 cells co-expressing mCherry-Ub and TDP-43-GFP or FUS-GFP. Related to Figure 4. The entire nucleus of NSC-34 cells co-expressing mCherry-Ub and TDP-43-GFP (A) or FUS-GFP (B) was photobleached and the recovery of Ub fluorescence was montitored. Pre-bleach, post-bleach and recovery endpoint (final read) are shown with the ROI (nucleus) marked by a solid white line. Scale bars: 10 μm.

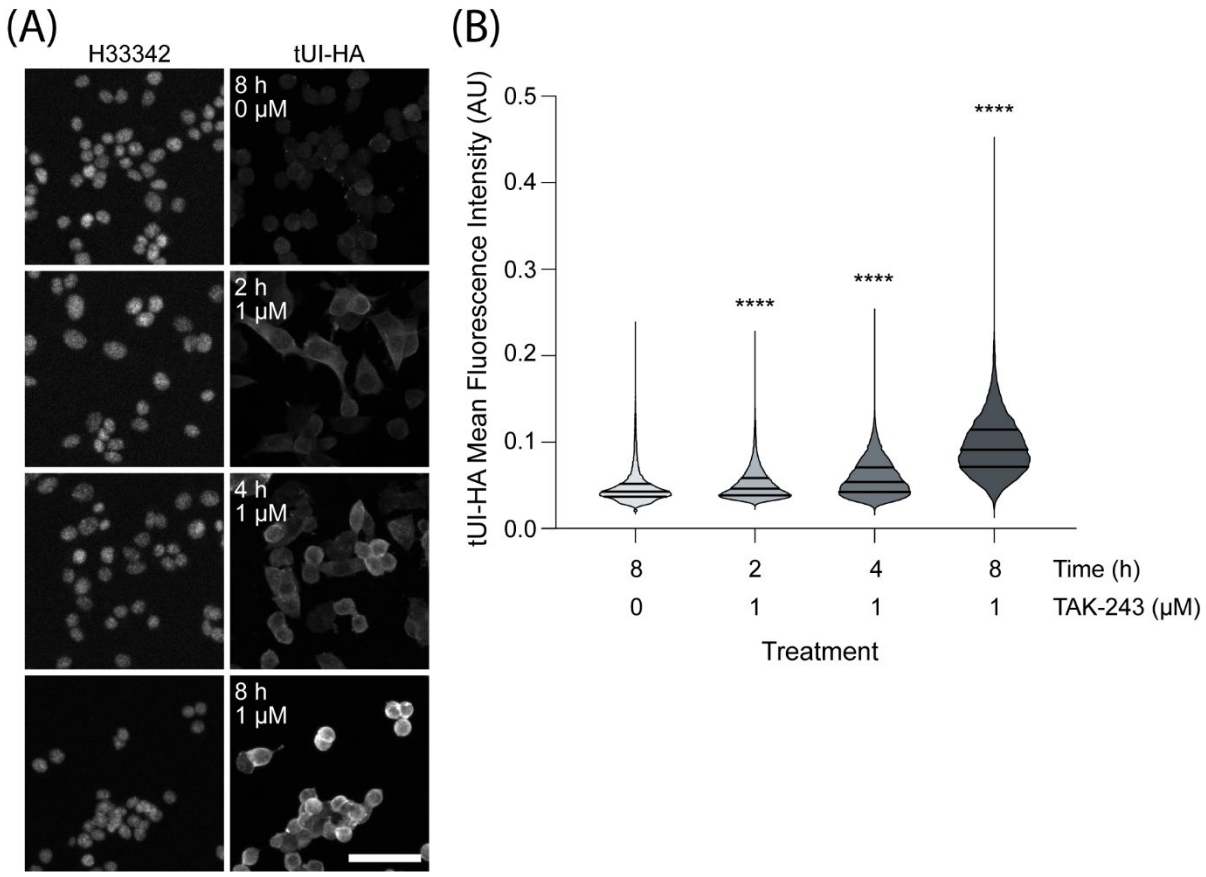

Figure S5. **tUI-HA detects free Ub in NSC-34 cells.** Related to Figure 5. (A) NSC-34 cells were fixed, permeabilised and stained for free Ub using the free Ub sensor tUI-HA (Choi et al., 2019) after incubation with the E1/UBA1 inhibitor TAK-243 (1μM) or DMSO control for the time period indicated. Scale bar represents 50 μm. (B) Violin plots of tUI-HA fluorescence in NSC-34 cells treated with TAK-243 quantified using CellProfiler analysis. Data shown includes the median, 75th quartile and 25th quartile with the width of the density plot indicating frequency (Vehicle; n = 15,423, 2 h; n = 14,815, 4 h; n = 17,667, 8 h; n = 19,082). Statistical significance was determined against vehicle control using a Kruskal-Wallis test with Dunn's multiple comparisons (**** = $p < 0.001$).

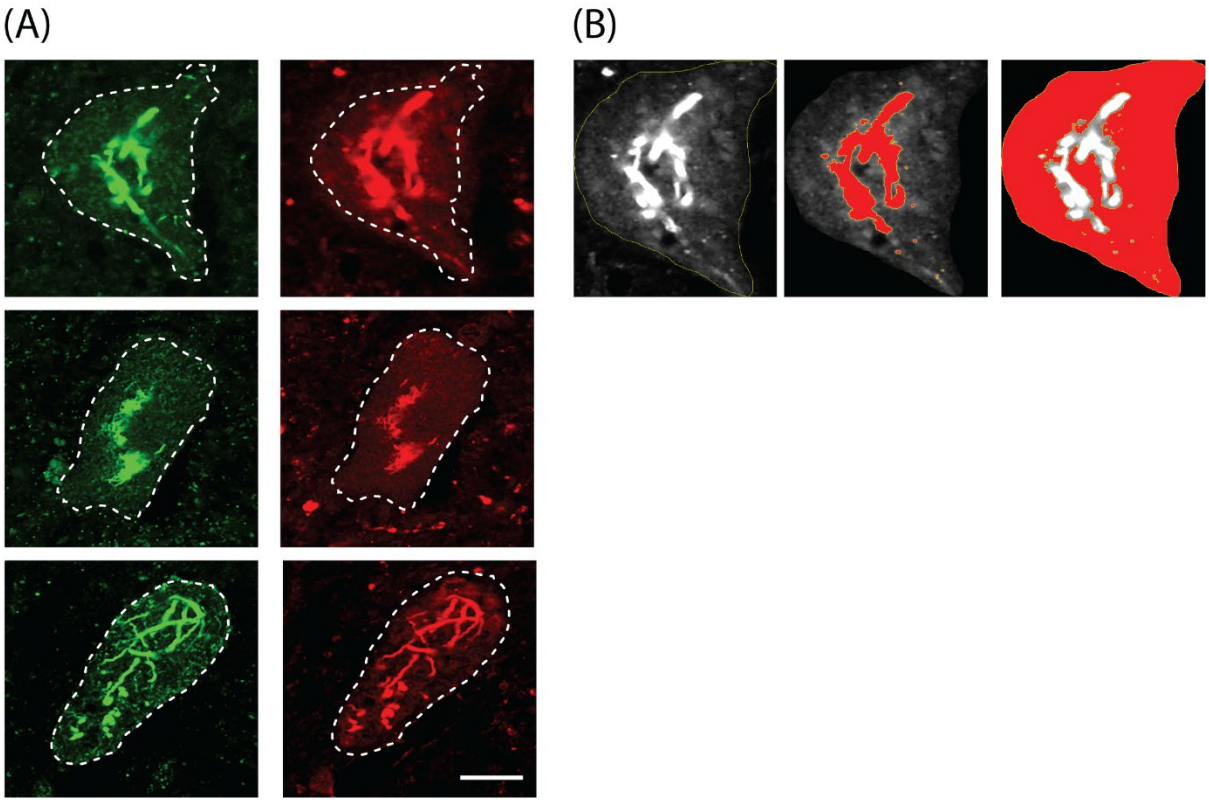

Figure S6. Human ALS post mortem tissue was stained for TDP-43 and Ub. Related to Figure 6. (A) Spinal cord motor neurons from sALS post mortem tissue probed with TDP-43 (green) and Ub (red) for evidence of perturbed Ub homeostasis. Cell outline marked by a dashed white line. Scale bar = 10 μm. (B) The intensity of Ub staining was calculated using ImageJ software (open source). The inclusion area was determined by setting a 'default' threshold and measuring the (pixel area and) mean pixel intensity. Diffuse (pixel area and) mean intensity were then measured by setting the maximum threshold to the value of the minimum threshold of an inclusion and setting a minimum threshold to a value that selects the remainder of the cell.

SUPPLEMENTAL TABLES

Table S1. UPS and autophagy related genes identified from the top 100 upregulated genes in ALS affected neurons relative to control neurons. Related to Figure 6.

Genes up regulated	**log2 (fold change)**	**Function**[a]
DDI1	*4.293*	*Seems to act as a proteasomal shuttle linking proteasome and replication fork proteins*
USP26	3.231	DUB[b]
UBE2C	2.466	E2 Ub conjugating enzyme
ASB11	*1.995*	*May be a substrate recognition component of a SCF[c]-like ECS[d] E3 ubiquitin ligase complex*
PSMB11	1.898	Proteasome subunit
IRGM	1.641	Regulates autophagy
RNF133	1.607	E3 Ub ligase
TRIM63	1.60	E3 Ub ligase
ASB5	*1.546*	*May be a substrate recognition component of a SCF-like ECS E3 ubiquitin ligase complex*
ZBTB16	*1.541*	*Probable substrate-recognition component of E3 Ub ligase complex*
UHRF1	1.42	E3 Ub ligase
MAP1LC3C	1.233	Ub-like modifier involved in xenophagy and aggrephagy
FBXO47	*1.193*	*Probably recognises phosphorylated proteins and promotes their ubiquitination*
KLHL10	*1.176*	*May be a substrate specific adaptor of a CUL3 based E3 Ub ligase*
DRAM1	1.148	Autophagy modulator
SOCS1	*1.142*	*Probable substrate recognition component of an ECS E3 Ub ligase*
TRIM22	1.12	E3 Ub ligase
DTL	1.067	Component of a DCX[e] E3 Ub ligase
ZNRF4	1.024	E3 Ub ligase
TRIM6	1.002	E3 Ub ligase
TRIM38	1.002	E3 Ub ligase
TRIM71	0.867	E3 Ub ligase
TRIM5	0.823	E3 Ub ligase
ZNF645	0.796	E3 Ub ligase
NEDD4	0.795	E3 Ub ligase
SOCS3	*0.793*	*Probable substrate recognition component of an ECS E3 Ub ligase*
RNF149	0.764	E3 Ub ligase
TRIM21	0.732	E3 Ub ligase
RNF135	0.721	E3 Ub ligase
DDB2	0.691	Substrate recognition module for DCX E3 Ub ligase complex
LRR1	*0.675*	*Probable substrate recognition subunit of an ECS E3 Ub ligase*
FBXL8	0.671	Substrate-recognition component of the SCF type E3 Ub ligase complex
ASB4	*0.661*	*Probable substrate recognition component of a SCF-like ECS E3 ubiquitin ligase complex*
HSPB8	0.657	Heat shock protein molecular chaperone
FBXO43	*0.591*	*Probably recognises phosphorylated proteins and promotes their ubiquitination*
FBXO39	0.578	Substrate-recognition component of the SCF type E3 Ub ligase complex
SOCS6	*0.577*	*May be a substrate recognition component of a SCF-like ECS E3 Ub ligase*
RNF19A	0.574	E3 Ub ligase
BIRC3	0.566	E3 Ub ligase
TNFAIP3	0.559	DUB and Ub ligase activity
PIAS1	0.554	Functions as an E3 type SUMO[f] ligase, promoting ubiquitin mediated degradation
TRIM4	0.528	E3 Ub ligase
TRIM47	0.522	E3 Ub ligase

TRIM29	0.519	Induces K48 ubiquitination
UBA7	0.504	E1 Ub activating enzyme

[a] All functions sourced from UniProtKB/Swiss-Prot, [b] DUB: deubiquitinating enzyme, [c] SCF: Skp-Cullin-F-box containing complex, [d] ECS: Elongin-Cullin-SOCS Box Complex, [e] DCX: E3 ligase composed of DDB1-CUL4-X-box, [f] SUMO: small ubiquitin like modifier. *Italicised genes are predicted to have roles in the UPS and/or autophagy.*

Table S2. UPS and autophagy related genes identified from the top 100 genes downregulated in ALS affected neurons relative to control neurons. Related to Figure 6.

Genes down regulated	**log2 (fold change)**	**Function**
ASB18	*-2.565*	*May be a substrate recognition component of a SCF-like ECS E3 ubiquitin ligase complex*
HECW1	-2.109	E3 Ub ligase
UCHL1	-1.867	DUB
RNF128	-1.735	E3 Ub ligase
USP6	-1.657	DUB
TRIM36	-1.383	E3 Ub ligase
LNX1	-1.360	E3 Ub ligase
FBXO16	*-1.314*	*Probably recognises phosphorylated proteins and promotes their ubiquitination*
TRIM58	-1.303	E3 Ub ligase
UBE2O	-1.197	E2 Ub conjugating enzyme
ZSWIM2	-1.193	E3 Ub ligase
FBXO41	-1.188	Substrate-recognition component of the SCF type E3 Ub ligase complex
FBXL16	-1.074	Substrate recognition component of a SCF-like ECS E3 ubiquitin ligase complex
NEDD4L	-1.03	E3 Ub ligase
CDC20	-0.992	Required for full Ub ligase activity of APC/C[b]
HECW2	-0.896	E3 Ub ligase
USP31	-0.884	DUB
MAP1LC3A	-0.862	Ub like modifier involved in formation of autophagosomes
USP5	-0.84	DUB
FBXO27	-0.781	Substrate recognition component of a SCF-like ECS E3 ubiquitin ligase complex
UBE2S	-0.776	E2 Ub conjugating enzyme
TRIM37	-0.761	E3 Ub ligase
TRIM2	-0.734	E3 Ub ligase
FBXL18	-0.703	Substrate recognition component of a SCF-like ECS E3 ubiquitin ligase complex
FBXO44	-0.701	Substrate recognition component of a SCF-like ECS E3 ubiquitin ligase complex
UBB	-0.640	Ubiquitin
HECTD4	-0.638	E3 Ub ligase
GABARAPL1	-0.637	Ub like modifier involved in formation of autophagosomes
USP35	-0.633	DUB
BTBD3	-0.630	Component of the 26S proteasome
PSMD12	-0.606	Component of the 26S proteasome
MAPK8IP1	-0.605	Regulator of autophagy
UBE2T	-0.598	E2 Ub conjugating enzyme
RNF165	-0.584	E3 Ub ligase
STUB1	-0.575	E3 Ub ligase
HSPA8	-0.560	Heat shock protein molecular chaperone
PSMB7	-0.555	Component of the 20S core proteasome
NHLRC1	-0.530	E3 Ub ligase

TRIM16	-0.526	E3 Ub ligase
PRPF19	-0.523	E3 Ub ligase
ATG4D	-0.498	Autophagy required protease
TRIM62	-0.498	E3 Ub ligase
UBE4B	-0.491	E3 Ub ligase
RNF187	-0.480	E3 Ub ligase
MAP1LC3B	-0.480	Ub like modifier involved in formation of autophagosomes
USP14	-0.480	DUB
PSMB5	-0.476	Component of the 20S core proteasome
TRIM41	-0.474	E3 Ub ligase
FBXL19	-0.472	Substrate recognition component of a SCF-like ECS E3 ubiquitin ligase complex
FBXO31	-0.471	Component of SCF like E3 ligase
CBX4	-0.469	E3 SUMO ligase
DCAF4	*-0.469*	*May function as a substrate receptor for CUL4-DDB1 E3 Ub ligase*
OTUB1	-0.467	DUB
PSMD8	-0.464	Component of the 26S proteasome
FBXL22	-0.457	Substrate-recognition component of the SCF type E3 Ub ligase complex
COPS5	-0.456	Regulator of Ub pathway by deneddylation os SCG-type E3 ligases
FBXL14	-0.455	Substrate-recognition component of the SCF type E3 Ub ligase complex
OTUB2	-0.453	DUB
PINK1	-0.452	Mediates mitophagy
RNF125	-0.452	E3 Ub ligase
ULK2	-0.445	Mediates autophagy
UBE2M	-0.444	E2 conjugating enzyme
ASB1	*-0.441*	*Probable substrate recognition component of a SCF-like ECS E3 ubiquitin ligase complex*
ULK1	-0.439	Mediates autophagy
UBE3C	-0.438	E3 Ub ligase
PSMD4	-0.438	Component of the 26S proteasome
ASB13	*-0.437*	*May be a substrate recognition component of a SCF-like ECS E3 ubiquitin ligase complex*
HSP90AA1	-0.436	Heat shock protein molecular chaperone

[a]: All functions sourced from UniProtKB/Swiss-Prot, [b] APC/C: Anaphase promoting complex/cyclosome. *Italicised genes are predicted to have roles in the UPS and/or autophagy*.

TRANSPARENT METHODS

Plasmids

Expression vector pCMV6-AC-tGFP containing human TDP-43 and FUS were obtained from OriGene (USA). mCherry-Ub and tdTomato^{CL1} constructs were generated as described previously (Farrawell et al., 2018). The tUI-HA construct to express tUI-HA protein in *Escherichia coli* was acquired from Addgene (Addgene plasmid 122662, deposited by Robert Cohen; (Choi et al., 2019)).

Antibodies

The following antibodies were used in this study: rabbit monoclonal against Ub^{K48} or Ub^{K63} polymers (05-1307/05-1308, Merck Millipore; 1:500 dilution), mouse monoclonal anti-Ub antibody (MAB1510, Chemicon; 1:100 dilution), mouse monoclonal anti-Ub antibody (sc-8017, Santa Cruz Biotechnology; 1:10,000 dilution), rabbit polyclonal anti-HA tag antibody (ab9110, Abcam; 1:1000 dilution), rabbit polyclonal anti-TDP-43 antibody (10782-2-AP, Proteintech; 1:1000 dilution), rabbit IgG polyclonal isotype control (ab171870, Abcam), Alexa Fluor 647-conjugated anti-rabbit-IgG secondary antibody (ab150079, Abcam; 1:1000 dilution), goat anti-mouse horseradish peroxidase conjugated secondary antibody (AP308P, Millipore; 1:5000 dilution).

Expression and purification of tUI-HA

Expression and purification of tUI-HA were carried out as reported previously (Choi et al., 2019) with alterations. The tUI-HA plasmid was transformed into chemically competent Rosetta BL21(DE3) pLysS cells using heat shock. Cells were grown in 2×YT medium to an optical density (600 nm) of 0.6 before expression was induced with 0.5 mM IPTG. After 8 hours of induction at 25 °C, cells were harvested by centrifugation at 3 200 ×*g* for 15 min at 4 °C and frozen at -20 °C until processing. Cell pellets were defrosted and resuspended in ice-cold lysis buffer (50 mM Tris, 500 mM NaCl, 30 mM Imidazole, 5 mM $MgSO_4$, 200 µg/mL Lysozyme, 10 µg/mL DNase, pH 8) supplemented with Complete EDTA-free protease inhibitor cocktail (Sigma). The resuspension was then incubated on ice for 30 min with gentle rocking prior to undergoing sonication on ice (30% amplitude, 20 sec on, 60 sec off, repeated 5 times). Sonicated suspensions were aspirated through a 22 gauge needle before cell debris was cleared via centrifugation at 40 000 ×*g* for 20 min at 4 °C. Cleared lysate was filtered through a 0.22 µm syringe filter before being deposited onto Ni-NTA resin in 50 mL falcon tubes (5 mL resin per 25 mL cell lysate). Ni-NTA resin with lysate was mixed via rotation (20 rpm) at 4 °C for 1 h. Following this, Ni-NTA resin was pelleted via centrifugation at 4000 ×*g* for 5 min at 4 °C. The supernatant was aspirated from the Ni-NTA resin, and the resin was washed with binding buffer 5 times (50 mM Tris, 500 mM NaCl, 30 mM Imidazole, pH 8) 5 times (25 mL binding buffer, 5 min equilibration, 4000 *g* for 5 min at 4 °C spins per wash). Following washing, the protein was dissociated from the Ni-NTA resin using 2 washes with 10 mL of dissociation buffer (50 mM Tris, 500 mM NaCl, 300 mM Imidazole, pH 8). The dissociated protein was checked for purity via reducing SDS-PAGE prior to being dialyzed. Dialysis occurred overnight in 5 L of 1× PBS at 4 °C with gentle stirring using SnakeSkin™ Dialysis Tubing, 3.5K MWCO (Thermofisher, USA). Dialyzed protein was filtered through a 0.22 µm syringe filter before being supplemented with glycerol (Sigma) to 15% (v/v) and TCEP (Sigma) to 0.5 mM. The concentration of the tUI-HA sensor was determined using UV/VIS spectroscopy (POLARStar Nano, BMG Labtech) at 280 nm using an extinction coefficient of 22920 $M^{-1}cm^{-1}$ to be 3mg/mL(M.Walker, 2005). The tUI-HA probe was aliquoted and flash-frozen in liquid nitrogen before being stored at -80 °C.

Cell culture and transfection

Mouse neuroblastoma × spinal cord hybrid NSC-34 cells (a kind gift from Professor Neil Cashman, University of British Columbia, Canada) (Cashman et al., 1992) were cultured in Dulbecco's Modified Eagle's Medium/Ham's Nutrient Mixture F12 (DMEM-F12) DMEM-F12 containing 10% FBS (Gibco) and were maintained at 37 °C in a humidified incubator with 5 % atmospheric CO_2. Cell were plated out on to multi-well plates or plastic 8-well µslides (Ibidi, Germany) at ~ 50 % confluency 24 h prior to transfection with Lipofectamine 3000 (Invitrogen, USA) or TransIT-X2 transfection reagent (Mirus Bio, USA). Transfections were carried out according to manufacturer's instructions. For co-transfections, the amount of DNA was divided equally between constructs.

Immunofluorescence

Staining of NSC-34 cells was performed according to Farrawell et al. (2018). NSC-34 cells grown on coverslips in 24-well plates were transfected with TDP-43-GFP or FUS-GFP and fixed 48 h post-transfection with 4% paraformaldehyde (PFA) in PBS for 20 min at room temperature (RT). Following permeabilization with 1 % Triton X-100 (TX-100) in PBS on ice for 30 min, cells were blocked with 5 % FBS, 1 % bovine serum albumin (BSA), 0.3 % TX-100 in PBS for 1 h at RT. Cells were then incubated

with primary antibodies against Ub^{K48} or Ub^{K63} polymers (1:500 dilution in 1 % BSA, 0.1 % TX-100 in PBS) overnight at 4 °C. The following day, cells were incubated with anti-rabbit IgG secondary antibody (1:500 dilution in 1 % BSA, 0.1 % TX-100 in PBS) for 5 h at RT before mounting coverslips onto slides using ProLong Diamond Antifade Mountant (Molecular Probes) and imaging on a Leica SP5 confocal microscope.
Immunostaining of post mortem tissue (obtained from the Australian Brain Bank Network) was performed as outlined previously (Farrawell et al., 2015). Spinal cord tissue sections (5 µm) from two sALS cases were treated with xylene and rehydrated with a series of decreasing dilutions of ethanol and water before antigen retrieval by heating in 10mM citrate buffer (pH 6.0). Sections were blocked with 1 % BSA before overnight incubation with primary antibodies (rabbit polyclonal anti-TDP-43 antibody (10782-2-AP, Proteintech) and mouse monoclonal anti-ubiquitin antibody (MAB1510, Chemicon)), followed by a 1 h incubation at RT with secondary antibodies (anti-rabbit conjugated Alexa Fluor 488 and anti-mouse conjugated Alexa Fluor 555). Confocal fluorescence imaging was performed using a Leica DM6000 upright laser scanning confocal microscope using Leica application suite advanced fluorescence software. Images were acquired with a 40× oil immersion objective in sequential mode to avoid crosstalk between two dyes.

Free Ub levels were measured in NSC-34 cells expressing TDP-43-GFP or FUS-GFP using the high-affinity free Ub sensor tUI-HA (Choi et al., 2019). Cells grown in 8-well µslides (Ibidi) were subjected to a short prefix step 48 h post-transfection with 2% PFA (pre-warmed to 37°C) for 5 min before fixing with 4% PFA at RT for 15 min. Cells were washed with 100 mM Tris pH 8.0 before permeabilization with 0.1% TX-100 in PBS. Cells were then blocked for 1 h at RT with blocking buffer (10% FBS, 2% BSA, 0.1% TX-100 in PBS) before incubating with the tUI-HA probe diluted 1:400 (7.5 µg/mL) in blocking buffer for 30 min at RT. Cells were incubated with anti-HA antibody in blocking buffer for 1 h at RT, or overnight at 4 °C, and washed three times with PBS before incubating with Alexa Fluor 647-conjugated secondary antibody in blocking buffer for 1 h at RT. Finally, cells were stained with ActinRed-555™ (Thermo Scientific) in PBS for 30 min at RT before being counterstained with Hoechst 33342 nucleic acid stain (diluted 1:5000 in PBS) for 5 min at RT, washed twice in PBS, and imaged using an SP8 confocal microscope. To determine the sensitivity and specificity of tUI-HA to free Ub, NSC-34 cells were treated (or not) with 1 µM of the E1/UBA1 inhibitor TAK-243 (ChemieTek, USA) for varying times (2, 4, or 8 h) prior to being fixed and stained with the tUI-HA probe as outlined above.

UPS activity assay
UPS activity was measured in cells expressing TDP-43-GFP or FUS-GFP using the fluorescent proteasome reporter $tdTomato^{CL1}$, as described previously (Farrawell et al., 2018). In summary, transfected NSC-34 cells were incubated with increasing concentrations (0 - 30 µM) of the proteasome inhibitor, MG132, for 18 h before harvesting 48 h post-transfection for analysis by flow cytometry on a LSRFortessa X-20 Cell Analyzer (BD Biosciences). The excitation wavelengths and collection windows used to measure the fluorescence intensity of tGFP and $tdTomato^{CL1}$ were 488 nm, 525/50 nm and 561 nm, 558/15 nm, respectively. Analysis was performed using FlowJo version 10 (FlowJo LLC, USA) and compensation was applied using the in-built compensation wizard before cells were gated based on tGFP fluorescence and the mean $tdTomato^{CL1}$ fluorescence was measured. Mean tdTomatoCL1 fluorescence was also measured in the untransfected (UT, GFP negative) population of cells co-transfected with tGFP to assess the impacts of MG132 treatment and the overexpression of a non-pathogenic protein on UPS function.

Confocal microscopy
Fluorescence recovery after photobleaching (FRAP) and fluorescence recovery after nuclear photobleaching (FRANP) experiments were performed on NSC-34 cells co-expressing mCherry-Ub and TDP-43-GFP or FUS-GFP 48 h post-transfection using the LASAF FRAP application wizard on an SP5 confocal microscope, as described previously (Farrawell et al., 2018). Briefly, to bleach mCherry-Ub, five pre-bleach 512 x 512 images were acquired over 7. 5 s using a 63× 1.2NA water-immersion objective at a scan speed of 700 Hz before the region of interest (ROI) was bleached using the 'zoom in ROI' method over five (1.5 s) frames with the 561 nm laser power set to 100%. Recovery of mCherry-Ub into the ROI was monitored over 120 s with the laser power set at 20%. For FRAP experiments, the ROI was set at ~ 2 µm in diameter in the nucleus or cytoplasm of cells.

To quantify tUI-HA staining, cells were imaged on an SP8 confocal (Leica) where Hoechst 33482 was excited with a 405 nm laser, Actin-555 was excited with a 552 nm laser, and Alexa Fluor 647 (tUI-HA) was excited with a 638 nm laser. Images (12-bit) were acquired using the 40× 1.3NA oil-immersion

objective, one line and frame average at a scan speed of 400 Hz. To segregate cells containing insoluble TDP-43^{M337V}-GFP inclusions or quantify tUI-HA fluorescence in cells treated with TAK-243, 16-bit resolution images in 1024 x 1024 format were acquired in 4 x 4 tilescans as z-stacks (17 slices or 20 µm) using the HC PL Fluotar 20× air objective (NA 0.55) with a scan speed of 200 Hz. Images were subsequently processed using CellProfiler software (Version 3.1.8) (McQuin et al., 2018) and ImageJ 1.52p (Schneider et al., 2012).

Image analysis for measuring Ub signal associated with inclusions
Image analysis to quantify the Ub signal associated with insoluble ALS-associated inclusions was performed using ImageJ software as described previously (Pokrishevsky et al., 2018). Briefly, the ROI within a cell consisting of aggregated TDP-43 or FUS was defined by setting a 'default' threshold in the GFP image. This ROI was subsequently applied to the mCherry image, and the mean pixel intensity was measured. The mean pixel intensity was also calculated for the remaining area of the cell containing diffuse protein by altering the maximum threshold in the GFP image to the minimum threshold set for the aggregated protein.

Quantification of tUI-HA fluorescence
A CellProfiler pipeline was developed to measure tUI-HA fluorescence in TDP-43-GFP and FUS-GFP expressing cells from images generated by the confocal microscope. Firstly, images were smoothed and then primary objects (nuclei) were identified based on size (10-50 pixel units) and minimum cross entropy thresholding. The nuclei were subsequently used to identify the secondary objects (cells) through propagation and adaptive thresholding in the ActinRed-555 channel. The GFP fluorescence intensity in the cells was then measured so they could be filtered to identify 'GFP positive' cells. Following filtering, tUI-HA fluorescence was measured in the 'GFP positive' cells, and the data was exported to a spreadsheet.

For cells treated with TAK-243, a separate CellProfiler pipeline was developed to produce max intensity and summed intensity projections of z-stacks for all images. Nuclei were identified using the StarDist plugin(Schmidt et al., 2018) for ImageJ using a script for batch processing. Stardist nuclei were used as primary objects in the CellProfiler pipeline where the whole cell was identified by propagation in the Actin-555 channel. Whole cell ROIs were applied to the tUI-HA images, and the mean intensity per cell was measured.

To measure tUI-HA fluorescence in cells containing insoluble TDP-43^{M337V}-GFP aggregates, summed intensity projections were generated using CellProfiler and subsequently manually processed using ImageJ software. Firstly, images from the GFP channel (TDP-43-GFP or FUS-GFP images) were thresholded to remove background, and the magic wand tool was used to manually segment cells and set ROIs based on fluorescence. These ROIs were applied to the tUI-HA images before the mean tUI-HA fluorescence intensity was measured.

Protein-Protein interactions
Protein-protein interactions and KEGG pathway analysis among the resulting protein list generated from microdissected ventral horn ALS spinal tissue (from D'Erchia et al. 2017) were analyzed using STRING (v10) (Szklarczyk et al., 2015) (with a confidence score of 0.700).

Cell lysis and fractionation
NSC-34 cells grown in 6-well plates were transfected with TDP-43-GFP, FUS-GFP or EGFP and harvested 48 h post-transfection with Trypsin/EDTA (Gibco). Cells were washed with PBS and each well was lysed in 100 µl of RIPA buffer [50mM Tris-HCl pH7.4, 1% (w/v) sodium deoxycholate, 150 mM NaCl, 1 mM EDTA, 1% (v/v) TX-100, 0.1% (w/v) SDS] containing protease inhibitors (Halt™ Protease Inhibitor Cocktail (Thermo Scientific)) and 10 mM N-Ethylmaleimide (NEM). Samples were briefly sonicated before centrifugation at 21 000 ×*g* at 4 °C for 1 h. The supernatant was collected as the 'soluble fraction' and the insoluble pellet was resuspended in urea buffer [7M Urea, 4% (w/v) CHAPS, 30 mM Tris pH 8.5] to create the 'insoluble fraction'. The insoluble fraction samples were sonicated in a sonicating waterbath for 10 min before protein concentration was determined using a BCA assay.

Western blotting
Soluble and insoluble fractions were reduced with 2.5% β-mercaptoethanol and heated for 10 mins at 70 °C. 15 µg of each sample was loaded and separated onto Any-kDa Mini-PROTEAN TGX Stain-Free precast gels (BioRad) and subsequently transferred onto PDVF membrane (0.2 µm pore size).

Membranes were imaged with a GelDoc XR+ imager (BioRad) to obtain a total protein measurement for each sample before incubation with blocking solution containing 5% skim milk powder (w/v) in Tris-Buffered Saline with Tween-20 (TBST) for 1 h at RT. Membranes were probed with mouse monoclonal anti-Ub antibody (sc-8017, Santa Cruz Biotechnology, 1:10,000 dilution in blocking buffer) overnight at 4 °C. Subsequently, membranes were incubated goat anti-mouse horseradish peroxidase-conjugated secondary antibody (AP308P, Millipore, 1:5000) for 1 h at RT. Bands were visualized by briefly incubating membrane in Amersham ECL Western blotting detection reagent (GE Healthcare) and imaged with Amersham 600RB Imager (GE Healthcare). Relative Ub levels for each sample were quantified using ImageJ gel analysis tools and normalized to their respective total protein measurement and an internal control sample (containing equal amounts of each sample), to account for protein loading and gel-to-gel variability.

Statistics

All statistical analyses were performed using GraphPad Prism software version 5.00 or 8.4.2 for Windows (GraphPad Software, USA). Specific details of analyses are provided in relevant figure captions.

SUPPLEMENTAL REFERENCES

CASHMAN, N. R., DURHAM, H. D., BLUSZTAJN, J. K., ODA, K., TABIRA, T., SHAW, I. T., DAHROUGE, S. & ANTEL, J. P. 1992. Neuroblastoma x spinal cord (NSC) hybrid cell lines resemble developing motor neurons. *Dev. Dyn.,* 194**,** 209-221.

M.WALKER, J. 2005. The Proteomics Protocols Handbook | Springer.

MCQUIN, C., GOODMAN, A., CHERNYSHEV, V., KAMENTSKY, L., CIMINI, B. A., KARHOHS, K. W., DOAN, M., DING, L., RAFELSKI, S. M., THIRSTRUP, D., WIEGRAEBE, W., SINGH, S., BECKER, T., CAICEDO, J. C. & CARPENTER, A. E. 2018. CellProfiler 3.0: Next-generation image processing for biology. *PLoS Biol.,* 16**,** e2005970.

POKRISHEVSKY, E., MCALARY, L., FARRAWELL, N. E., ZHAO, B., SHER, M., YERBURY, J. J. & CASHMAN, N. R. 2018. Tryptophan 32-mediated SOD1 aggregation is attenuated by pyrimidine-like compounds in living cells. *Sci. Rep.,* 8**,** 15590.

SCHMIDT, U., WEIGERT, M., BROADDUS, C. & MYERS, G. 2018. Cell Detection with Star-Convex Polygons. *Medical Image Computing and Computer Assisted Intervention - Miccai 2018, Pt Ii,* 11071**,** 265-273.

SCHNEIDER, C. A., RASBAND, W. S. & ELICEIRI, K. W. 2012. NIH Image to ImageJ: 25 years of image analysis. *Nat Methods,* 9**,** 671-5.

SZKLARCZYK, D., FRANCESCHINI, A., WYDER, S., FORSLUND, K., HELLER, D., HUERTA-CEPAS, J., SIMONOVIC, M., ROTH, A., SANTOS, A., TSAFOU, K. P., KUHN, M., BORK, P., JENSEN, L. J. & VON MERING, C. 2015. STRING v10: protein-protein interaction networks, integrated over the tree of life. *Nucleic Acids Res,* 43**,** D447-52.